Passive Walking Biped Robot Model with Flexible Viscoelastic Legs

Masoumeh Safartoobi
Babol Noshirvani University of Technology
HamidReza Mohammadi Daniali
Babol Noshirvani University of Technology
Morteza Dardel (dardel@nit.ac.ir)
Babol Noshirvani University of Technology https://orcid.org/0000-0002-5206-508X

Research Article

Keywords: Passive walking, biped, flexible, viscoelastic leg, gait

Posted Date: November 15th, 2021

DOI: https://doi.org/10.21203/rs.3.rs-1000853/v1

Passive walking biped robot model with flexible viscoelastic legs

Masoumeh Safartoobi [(a)], Hamidreza Mohammadi Daniali [(a)] and Morteza Dardel[1(a)]

(a) Department of Mechanical Engineering, Babol Noshirvani University of Technology

Abstract

To simulate the complex human walking motion accurately, a suitable biped model has to be proposed that can significantly translate the compliance of biological structures. In this way, the simplest passive walking model is often used as a standard benchmark for making the bipedal locomotion so natural and energy-efficient. This work is devoted to a presentation of the application of internal damping mechanism to the mathematical description of the simplest passive walking model with flexible legs. This feature can be taken into account by using the viscoelastic legs, which are constituted by the Kelvin–Voigt rheological model. Then, the update of the impulsive hybrid nonlinear dynamics of the simplest passive walker is obtained based on the Euler–Bernoulli's beam theory and using a combination of Lagrange mechanics and the assumed mode method, along with the precise boundary conditions. The main goal of this study is to develop a numerical procedure based on the new definition of the step function for enforcing the biped start walking from stable condition and walking continuously. The study of the influence of various system parameters is carried out through bifurcation diagrams, highlighting the region of stable period-one gait cycles. Numerical simulations clearly prove that the overall effect of viscoelastic leg on the passive walking is efficient enough from the viewpoint of stability and energy dissipation.

Keywords: Passive walking, biped, flexible, viscoelastic leg, gait.

1. Introduction

Studying passive bipedal walking is a fascinating field in the research of legged walking robots for its achievement in human locomotion mimicry. Passive dynamic walking is one of the locomotion strategies which can settle into a stable steady and symmetric gait on a gentle slope without requiring any active control using gravity and dynamic nature of the swing leg [1]. It is clear that the passive walking gait is highly energy efficient and thus,

[1]Corresponding author: Department of Mechanical Engineering, Babol Noshirvani University of Technology, P.O. Box 484, Postal Code: 47148-71167, Shariati Street, Babol, Mazandaran, Iran. dardel@nit.ac.ir, mdardel@gmail.com.

investigating these natural gaits may lead us to gain a deeper understanding of human and insects walking.

From the mathematical point of view, the complex impulsive hybrid nonlinear dynamics of the passive walking is influenced greatly due to changes of the biped robot model parameters. Therefore, optimal designs of passive walkers are one of the controversial topics that have been attracted a lot of interest. Two well-known passive bipeds with simple mechanical structure, the compass-like biped robot and the point-foot walker were then conceived by Goswami et al. [2] and Garcia et al. [3], respectively. They have numerically showed the existence of stable period-one gait cycles on a range of steeper slopes and then the cascade of period-doubling bifurcations as a route to chaos by varying the slope angle and even the structural parameters of the models [4-6]. After that, many follow-on robotic scholars have performed studies on the most popular passive walkers with knees [7], with a torso on hip [8], with different foot shapes [9,10], with stabilizing arm [11], by changing walking ramp surface into stairs [12] and also by considering the friction forces [13]. In recent years, considerable research works conducted under the passive dynamic walking are mainly an analysis of its dynamic characteristics, namely limit cycle, Poincaré map, stability, bifurcations, chaos, control and so on, as in [14-26], just to mention a few. The interested readers are also referred to the papers in [27,28] for an extensive treatment of design and dynamic analyses of various passive and semi-passive biped walkers. It is worth noting that many excellent theoretical and experimental results are achieved in these literatures.

In the strive for simulating passive elastic mechanisms utilized in human walking, a group of researchers has decided to use compliant elements at different positions of the rigid biped such as torsional spring in joints [29], ankle [30] and torsional stiffness in the hip joint [31]. An extended model of the compass-gait biped with series-elastic ankle actuation was investigated in [32] which exhibited asymptotically stable walking on flat ground. The spring added to the ankle joint of the stance leg is stimulated toe push-off like human. Deng et al [33] studied the walker's specifications by adding a fully passive torso to a passive biped via torsional springs. The presented results showed two stable gait cycles with different properties and also improvements in gait performances. A chaotic particle swarm optimization algorithm was applied by Wu et al [34] to the optimal design of passive walker with hip torsional stiffness and damping at multi-variable level. A modified model of Garcia's basic passive biped with a sole foot and a combination of elastic and viscous elements at both hip and ankle joints was presented in [35]. By studying nonlinear dynamics and chaotic behavior of this biped model, the authors observed two possible patterns of motion similar to multi-pattern humanoid gait and also investigated the influence of system parameters on the stability of motion. These examples have been proven that adding elastic elements to the biped based on biomechanical compliance has advantages over the rigid link walker; however, it requires more sophisticated nonlinear mathematics to describe the impulsive hybrid passive dynamic walking and increases the designing leg mechanism complexity as anticipated.

In addition to the benefits of the local compliant elements in hard-bodied bipedal robots, there is still a gap between the structure of walkers and the human anatomy from a technical robotic design perspective. In contrast to the conventional rigid legs, the intrinsically flexible nature and extensible materials of the physical structure can mimic the properties of the biological tissues and muscles of the human leg and then the passive

walker appears more realistic. Therefore, using light-weight flexible legs can help the walker generate natural and very efficient walking pattern, adapt to uneven terrains and increase adaptability. Nevertheless, there are few researches dedicated to the flexible passive walkers having elastic legs instead of rigid links. For instance, Shen et al [36] have studied walking dynamic responses, complicated contact modes and impact-induced waves of a new compliant biped robot on an elastic walking surface. Great attention of this work has to be placed on the effects of sliding contact such as dynamic self-locking phenomenon on walking stability of the compliant walker. The other research work in [37], our earlier study, developed a modified flexible model of the Garcia's simplest passive walker with elastic legs. The unwanted vibrations induced by these undamped legs exhibited non-periodic gait cycle. After adding damping, we found proper initial conditions for period-one gait cycles and then investigated the influences of the walker's parameters through bifurcation diagrams.

It is observed that in the above cited references, the energy dissipation of the pure elastic legs was either ignored or considered as a simple viscous damping, while, in practice, due to the internal damping forces, the vibrations are damped. It turns out that it is highly desirable to use passive damping technology for flexible legs with simple computational tasks. A common way to minimize undesired vibrations in structures such as flexible manipulators [38] is to use viscoelastic materials. Hence, these simple, inexpensive and widely available materials are the best biomechanical models like artificial muscles to get a good design of high-performance passive walkers. To the best of authors' knowledge, no previous study has been made to utilize inherently dissipative materials in known passive walkers. Consequently, the present paper aims to implement the intrinsic viscoelastic properties of muscles in flexible passive biped robots in order to enhance the natural look of walking and deal with vibrations of the former elastic legs. Following our recent study in [37], the main contributions of this paper lie in modeling the flexible simplest passive walker, numerically finding proper initial motion state for its period-one gait cycles and discussing the effect of specific parameters on walking manner, but by proposing the viscoelastic legs.

The remaining part of this article is organized as follows. Section 2 presents the mechanics model, the corresponding formulation as well as the process of obtaining suitable initial conditions for stable walking. In Section 3, the results of numerical simulations and comparisons are given and discussed. Finally, Section 4 is devoted to the concluding remarks.

2. Walking pattern analysis

The simulation of one step comprises swing phase, a heel-strike collision and a set of discrete update laws. Relying on the author's study in [37], the goal of this section is to give a brief overview of the simulation procedure for one walking step of the flexible simplest passive walker with viscoelastic legs. Besides many similarities with elastic legs, using the viscoelastic legs will lead to have new assumptions. The following procedure is fully documented in [37] and the interested readers are referred to this publication for a comprehensive study.

2.1. Dynamic modeling

2.1.1. Physical description

Fig. 1 illustrates the Garcia's simplest walking model [3], a standard benchmark for studying periodic gaits and the modified flexible model. The new introduced model consists of two identical compliant legs, connected by a frictionless hip joint of point mass *M* that allows for rotational motion in the 2-D plane. The significant physical parameters and using variables for the numerical simulation have been shown in Fig. 1.

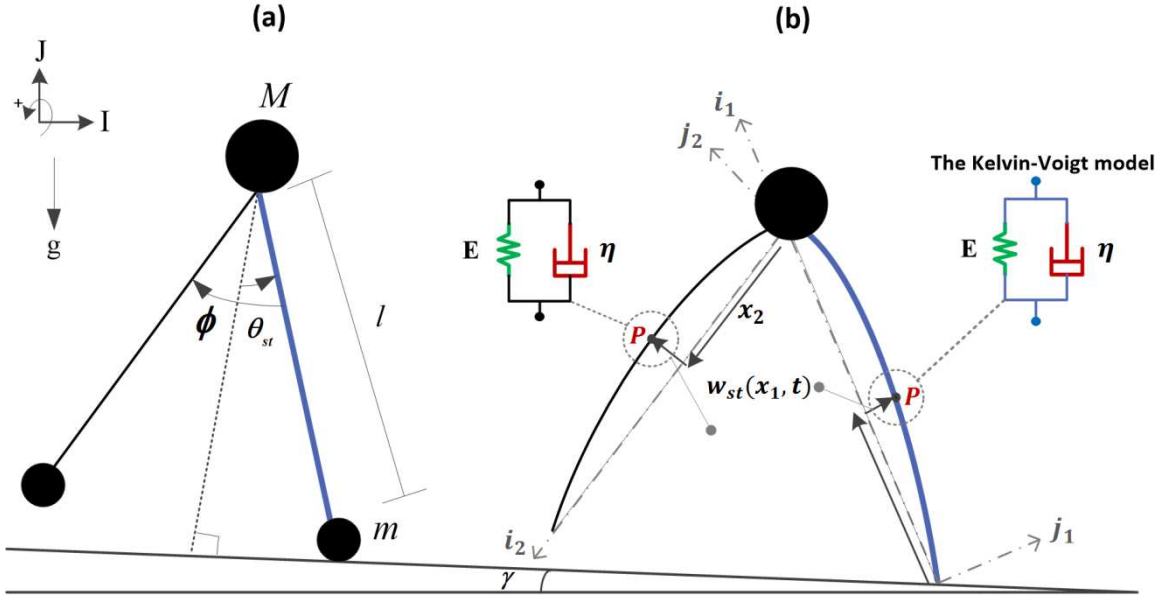

Figure 1: (a) Simplest walking model, (b) modified model with viscoelastic legs.

The legs are considered to have homogeneous material properties with same length L, mass density ρ, moment of inertia I and constant circular cross sectional area A. Using the classical Euler–Bernoulli beam theory and including the structural viscoelastic effect, the slender legs of the walker are modeled based on the bending mechanism of flexible links. The key kinematic assumptions made for the convenient analysis of deformations are as follows

(a) For each leg, the centerline of cross section is inextensible.
(b) During deformation, the cross section area is assumed to remain planar and normal to the deformed axis of the leg.
(c) Shear deformation, rotary inertia, the nonlinear geometric effect due to bending and warping are negligible.
(d) Each leg undergoes small deflection.
(e) The flexible legs with Young's modulus E and viscosity coefficient η obey the Kelvin–Voigt rheological model.

The total deformation of each leg is composed of rigid rotation due to the angles θ and ϕ and transverse displacement of neutral axis. The position vectors in the local coordinate systems denoting an arbitrary point P of the cross-sections of two legs are represented by

$$\overrightarrow{r_{P_{st}}} = x_1\hat{\imath}_1 + w_{st}(x_1,t)\hat{\jmath}_1 \quad , \quad \overrightarrow{r_{P_{sw}}} = x_2\hat{\imath}_2 + w_{sw}(x_2,t)\hat{\jmath}_2 \qquad (1)$$

where $w_{st}(x_1, t)$ and $w_{sw}(x_2, t)$ are the transverse displacements of the neutral axis (at point x and time t) compatible with the bending of the flexible legs. In this manuscript, the subscripts st and sw indicates the stance leg and the swing leg respectively.
The whole movement process is a repetition of consecutive gaits constrained in two phases: a swing phase and an impact phase. Such kind of walking is started by launching the robot with a wise choice of initial conditions and the angle of the ramp. During a step, the stance leg is modeled as a hinge, connected to the floor. The swing leg is moving freely as the other end of a double pendulum. At about midstance, the swing leg will experience an impact with the ground (scuffing), which is inevitable for a walker with equal leg lengths. However, the scuffing problem of the swing leg is neglected in the theoretical study and there is no slip and no bounce at the contact point. Practically, leg shortening measure mechanisms such as a prismatic-jointed knee [39] would solve the scuffing problem without affecting the walker dynamics. After this short through-pass, the second time that the swing leg reaches floor level is regarded as heel-strike, the end of the step. The former swing leg makes a fully inelastic collision and becomes the new stance leg. Instantaneously, the former stance leg loses ground contact, and a new step begins. Similar to the traditional rigid simplest passive walker, the flexible leg of this modified model is in point contact with the surface during the walking process.

2.1.2. Derivation the equations of the swing motion

The continuous dynamics of the passive walker as it travels down a shallow slope describes the bipedal motion between collisions and hence it is represented by a set of nonlinear differential equations. These swing equations of the viscoelastic Euler–Bernoulli legs, a set of coupled partial differential equations (PDE) and ordinary differential equations (ODE) along with the corresponding boundary conditions are derived using the extended Hamilton principle. First, the kinetic and potential energy and also the dissipated energy due to the damping effects should be obtained.
The position vectors of point P located at distances x_1 and x_2 from the local frame origins of the legs with respect to the contact point of the stance leg in the inertial coordinate system are given by

$$\vec{r}_{P_{st}} = [w_{st}(x_1, t)\cos(\theta_{st} - \gamma) - x_1 \sin(\theta_{st} - \gamma)]\hat{I} + [w_{st}(x_1, t)\sin(\theta_{st} - \gamma) + x_1 \cos(\theta_{st}(t) - \gamma)]\hat{J}$$

$$\vec{r}_{Hip} = \left[w_{st_l} cos(\theta_{st} - \gamma) - l\sin(\theta_{st} - \gamma)\right]\hat{I} + \left[w_{st_l}\sin(\theta_{st} - \gamma) + l\cos(\theta_{st} - \gamma)\right]\hat{J} \quad (2)$$

$$\vec{r}_{P_{sw}} = \vec{r}_{Hip} + [-w_{sw}(x_2, t)\cos(\theta_{st} - \phi - \gamma) + x_2 \sin(\theta_{st} - \phi - \gamma)]\hat{I} + [-w_{sw}(x_2, t)\sin(\theta_{st} - \phi - \gamma) - x_2 \cos(\theta_{st} - \phi - \gamma)]\hat{J}$$

The subscript l denotes the value of the $w_{st}(x, t)$ at $= l$, i.e. $w_{st}(l, t)$.
The total kinetic energy of the system can thus be expressed as

$$
\begin{aligned}
\mathrm{T} = {} & \frac{1}{2}\rho A \int_0^l \left[\left(\frac{\partial w_{st}(x_1,t)}{\partial t} \right)^2 - 2x_1 \frac{\partial w_{st}(x_1,t)}{\partial t} \dot{\theta}_{st} + (x_1^2 + w_{st}^2(x_1,t)) \dot{\theta}_{st}^2 \right] dx_1 \\
& + \frac{1}{2}\rho A \int_0^l \left\{ \left(l^2 + w_{st_l}^2 \right) \dot{\theta}_{st}^2 - 2 \left[l \frac{\partial w_{st}(l,t)}{\partial t} \dot{\theta}_{st} + x_2 \frac{\partial w_{sw}(x_2,t)}{\partial t} \left(\dot{\theta}_{st} - \dot{\phi} \right) \right] \right. \\
& \left. + \left(x_2^2 + w_{sw}^2(x_2,t) \right) \left(\dot{\theta}_{st} - \dot{\phi} \right)^2 + \left(\frac{\partial w_{st}(l,t)}{\partial t} \right)^2 + \left(\frac{\partial w_{sw}(x_2,t)}{\partial t} \right)^2 \right\} dx_2 \\
& + \frac{1}{2} M \left[\left(\frac{\partial w_{st}(l,t)}{\partial t} \right)^2 - 2l \frac{\partial w_{st}(l,t)}{\partial t} \dot{\theta}_{st} + \left(l^2 + w_{st_l}^2 \right) \dot{\theta}_{st}^2 \right]
\end{aligned}
\tag{3}
$$

The potential energy of each flexible leg arises from two sources, gravity and internal bending moment. From the mechanics of materials, bending moment in an arbitrary cross-section is approximated by

$$
M \approx EI \frac{\partial^2 w(x,t)}{\partial x^2} \tag{4}
$$

Then, the simplified form of the total potential energy of the system can be formulated as

$$
\begin{aligned}
U = {} & \rho A g \left\{ \int_0^l \left[w_{st}(x_1,t) \sin(\theta_{st} - \gamma) + x_1 \cos(\theta_{st} - \gamma) \right] dx_1 \right. \\
& + \int_0^l \left[w_{st_l} \sin(\theta_{st} - \gamma) \right. \\
& \left. \left. + l \cos(\theta_{st} - \gamma) - w_{sw}(x_2,t) \sin(\theta_{st} - \phi - \gamma) - x_2 \cos(\theta_{st} - \phi - \gamma) \right] dx_2 \right\} \\
& + \frac{1}{2} \int_0^l EI \left(\frac{\partial^2 w_{st}(x_1,t)}{\partial {x_1}^2} \right)^2 dx_1 + \frac{1}{2} \int_0^l EI \left(\frac{\partial^2 w_{sw}(x_2,t)}{\partial {x_2}^2} \right)^2 dx_2 \\
& + Mg \left[w_{st_l} \sin(\theta_{st} - \gamma) + l \cos(\theta_{st} - \gamma) \right]
\end{aligned}
\tag{5}
$$

The constitutive law of the classical Kelvin–Voigt model for the viscoelastic material is

$$
\sigma = E\varepsilon + \eta\dot{\varepsilon} \tag{6}
$$

where $\dot{\varepsilon}$ is the extensional strain rate. Using Eq. (6) and defining the bending moment in terms of stress, the non-conservative force of the viscoelastic beam is

$$
F_{nc} = \int_0^l \eta I \frac{\partial}{\partial t} \left(\frac{\partial^4 w(x,t)}{\partial x^4} \right) dx \tag{7}
$$

Therefore, the total virtual work done by this non-conservative force for the legs may be written as

$$
W_{nc} = -\eta I \left[\int_0^l \frac{\partial}{\partial t} \left(\frac{\partial^4 w_{st}(x_1,t)}{\partial x_1^4} \right) dx_1 + \int_0^l \frac{\partial}{\partial t} \left(\frac{\partial^4 w_{sw}(x_2,t)}{\partial x_2^4} \right) dx_2 \right] \tag{8}
$$

Now, the generalized Hamilton principle takes the form

$$\int_{t_1}^{t_2} (\delta \mathcal{L} + \delta W_{nc}) dt = 0 \tag{9}$$

where $\mathcal{L} = T - U$. Substitution the variation principle of Eq. (3), Eq. (5) and Eq. (8) into Eq. (9) leads to yield the nonlinear differential equations of motion as

$$\begin{aligned}
&\rho A \left\{ \int_0^l \left(g w_{st} \cos(\theta_{st} - \gamma) - x_1 \ddot{w}_{st} + w_{st}^2 \ddot{\theta}_{st} + 2 w_{st} \dot{w}_{st} \dot{\theta}_{st} \right) dx_1 \right. \\
&\quad + \int_0^l \left(g \left[w_{st_l} \cos(\theta_{st} - \gamma) - w_{sw} \cos(\theta_{st} - \phi - \gamma) \right] + w_{st_l}^2 \ddot{\theta}_{st} + 2 w_{st_l} \dot{w}_{st_l} \dot{\theta}_{st} \right. \\
&\quad \left. \left. - l \ddot{w}_{st_l} - x_2 \ddot{w}_{sw} + w_{sw}^2 \left(\ddot{\theta}_{st} - \ddot{\phi} \right) + 2 w_{sw} \dot{w}_{sw} \left(\dot{\theta}_{st} - \dot{\phi} \right) \right) dx_2 \right\} \\
&\quad + \rho A g \frac{l^2}{2} \left[-3 \sin(\theta_{st} - \gamma) + \sin(\theta_{st} - \phi - \gamma) \right] + \rho A \frac{l^3}{3} \left(5 \ddot{\theta}_{st} - \ddot{\phi} \right) \\
&\quad + M \left\{ g \left[w_{st_l} \cos(\theta_{st} - \gamma) - l sin(\theta_{st} - \gamma) \right] + \left(l^2 + w_{st_l}^2 \right) \ddot{\theta}_{st} + 2 w_{st_l} \dot{w}_{st_l} \dot{\theta}_{st} \right. \\
&\quad \left. - l \ddot{w}_{st_l} \right\} = 0
\end{aligned} \tag{10}$$

$$\begin{aligned}
&\rho A \left\{ \int_0^l \left[g w_{sw} \cos(\theta_{st} - \phi - \gamma) + x_2 \ddot{w}_{sw} - w_{sw}^2 \left(\ddot{\theta}_{st} - \ddot{\phi} \right) \right. \right. \\
&\quad \left. \left. - 2 w_{sw} \dot{w}_{sw} \left(\dot{\theta}_{st} - \dot{\phi} \right) \right] dx_2 \right\} - \rho A g \frac{l^2}{2} \sin(\theta_{st} - \phi - \gamma) + \rho A \frac{l^3}{3} \left(\ddot{\theta}_{st} - \ddot{\phi} \right) = 0
\end{aligned} \tag{11}$$

$$EI \frac{\partial^4 w_{st}}{\partial x_1^4} + \eta I \frac{\partial^4 \dot{w}_{st}}{\partial x_1^4} - \rho A \left[w_{st} \dot{\theta}_{st}^2 - \left(\ddot{w}_{st} - x_1 \ddot{\theta}_{st} \right) - g sin(\theta_{st} - \gamma) \right] = 0 \tag{12}$$

$$\begin{aligned}
&EI \frac{\partial^4 w_{sw}}{\partial x_2^4} + \eta I \frac{\partial^4 \dot{w}_{sw}}{\partial x_2^4} \\
&\quad - \rho A \left[w_{sw} \left(\dot{\theta}_{st} - \dot{\phi} \right)^2 - \ddot{w}_{sw} + x_2 \left(\ddot{\theta}_{st} - \ddot{\phi} \right) + g sin(\theta_{st} - \phi - \gamma) \right] = 0
\end{aligned} \tag{13}$$

and the leg's boundary conditions are described as:
at $x_1 = 0$

$$w_{st}(0, t) = 0 \quad , \quad EI \left. \frac{\partial^2 w_{st}(x_1, t)}{\partial x_1^2} \right|_{x_1 = 0} = 0 \tag{14}$$

at $x_1 = l$

$$\begin{aligned}
&EI \left. \frac{\partial^3 w_{st}(x_1, t)}{\partial x_1^3} \right|_{x_1 = l} + \rho A l \left[w_{st_l} \dot{\theta}_{st}^2 - g sin(\theta_{st} - \gamma) - \ddot{w}_{st_l} + l \ddot{\theta}_{st} \right] + M \left[w_{st_l} \dot{\theta}_{st}^2 - \right. \\
&\left. g sin(\theta_{st} - \gamma) - \ddot{w}_{st_l} + l \ddot{\theta}_{st} \right] = 0
\end{aligned} \tag{15}$$

$$EI\left.\frac{\partial^2 w_{st}(x_1,t)}{\partial x_1^2}\right|_{x_1=l}=0$$

at $x_2=0$

$$w_{sw}(0,t)=0 \quad , \quad \left.EI\frac{\partial^2 w_{sw}(x_2,t)}{\partial x_2^2}\right|_{x_2=0}=0 \tag{16}$$

at $x_2=l$

$$\left.EI\frac{\partial^2 w_{sw}(x_2,t)}{\partial x_2^2}\right|_{x_2=l}=0 \quad , \quad \left.EI\frac{\partial^3 w_{sw}(x_2,t)}{\partial x_2^3}\right|_{x_2=l}=0 \tag{17}$$

As expected, according to the equations in [37], viscoelastic legs affect only deformation equations as seen in Eq. (12) and Eq. (13). The resolution of the resulting continuous dynamics containing four coupled PDE and ODE is a challenging mathematical problem to solve analytically and computationally. To overcome, the assumed modes method (AMM), one of the popular formulation techniques for converting the PDE into ODE, is adopted here to perform the discretization of the developed equations.

We are interested now in using a combined Euler-Lagrange formulation and AMM to obtain the temporal equations of the swing motion. Accordingly, the approximate deflection subject to transverse vibrations of an elastic beam is expanded in a finite series of the form as [40]

$$w_{st}(x_1,t)=\sum_{i=1}^{n}\varphi_i(x_1)v_i(t) \quad , \quad w_{sw}(x_2,t)=\sum_{i=1}^{n}\psi_i(x_2)p_i(t) \tag{18}$$

where $\varphi_i(x_1)$ and $\psi_i(x_2)$ are the admissible functions that must satisfy the simply supported-free boundary conditions [41] relying on the geometric boundary conditions in Eq. (11) and n is the number of modes assumed in the approximation. Indeed, the stance leg and the swing leg are fixed to the contact point on the walking surface and the hip joint, respectively, while the other end of both legs is free. $v_i(t)$ and $p_i(t)$ are the time-dependent modal generalized coordinates and n is the number of modes.

By inserting the discrete formulation of determined kinetic energy and potential energy in Eq. (3) and Eq. (5) as well as the virtual work of non-conservative damping force in Eq. (8) into the Lagrange's equation [2], which may be written as below,

$$\frac{d}{dt}\left(\frac{\partial T}{\partial \dot{q}_i}\right)-\left(\frac{\partial T}{\partial q_i}\right)+\left(\frac{\partial U}{\partial q_i}\right)=Q_i \qquad i=1,2,\dots,(2n+2) \tag{19}$$

the reduced equations of motion written in terms of the generalized coordinates $\boldsymbol{q}$ are

$$\boldsymbol{M}(\boldsymbol{q})\ddot{\boldsymbol{q}}=\boldsymbol{F}(\boldsymbol{q},\dot{\boldsymbol{q}})+\boldsymbol{F_v}(\dot{\boldsymbol{q}}) \tag{20}$$

where $\boldsymbol{q}=[\theta_{st}\ \ v_1\dots v_n\ \ \phi\ \ \ p_1\dots p_n]^T$ is the vector of generalized coordinates whose variables are functions of dimensionless time $\tau=t\sqrt{\frac{g}{l}}$. $\boldsymbol{M}$ is the inertia matrix, $\boldsymbol{F}$ represents

a global force vector, a vector of gravity forces and also includes the centrifugal and coriolis terms and $\boldsymbol{F_v}$ is the vector of viscous structural damping term. Eq. (18) results two sets of nonlinear time varying coupled, second order ordinary differential equations in the matrix form. The first set of these equations is associated with the rigid rotation of the flexible legs defined by θ and ϕ, and it is quite identical for both elastic and viscoelastic; the other set is associated with the elastic deformation defined by v_i and p_i and it slightly differs from the given equations of the pure elastic legs in [37].
To transform the governing equations into dimensionless form and generalize the research results, the following dimensionless parameters are introduced as

$$\bar{x} = \frac{x}{l}\ , \bar{v} = \frac{v}{l}\ , \bar{p} = \frac{p}{l}\ \ , \quad \bar{M} = \frac{M}{\rho A l}\ \ , \quad D = \frac{EI}{\rho A g l^3}\ \ , \quad \bar{\eta} = \frac{\eta}{E}\sqrt{\frac{g}{l}} \tag{21}$$

Under the AMM and retaining a finite number, n = 1 mode, upper triangular dimensionless components of the inertia matrix and the non-zero vectors $\boldsymbol{F}$ and $\boldsymbol{F_v}$ in Eq. (20) are derived in Appendix A.

2.1.3. Transition rules at impact conditions

In order to describe what happens to the walker during heel-strike, transition rules must be formulated to prevent trespassing of the surface slope during motion. Heel-strike collision is modeled as a rigid plastic impact with immediate and full contact to the floor. When the swing leg hits the surface, an instantaneous transition occurs where the previous stance leg loses contact and the stance and swing leg switch. After this transition, the biped will be in the exact same configuration as shown in Fig .1.(a) with the exception that the generalized coordinates θ and ϕ have switched places. Moreover, an update of the angular velocities should occur to prevent the walker from falling through the floor. These changes in leg position states and their velocities are algebraic equations which called transition rules as given below

$$\begin{Bmatrix} \boldsymbol{q} \\ \dot{\boldsymbol{q}} \end{Bmatrix}^{+} = \begin{bmatrix} \boldsymbol{J} & 0 \\ 0 & \boldsymbol{H} \end{bmatrix} \begin{Bmatrix} \boldsymbol{q} \\ \dot{\boldsymbol{q}} \end{Bmatrix}^{-} \tag{22}$$

where the − and + signs denote the time instant right before and right after impact, respectively.
Following our recent study in [37], the above procedure of heel-strike collision happened in the rigid passive walker will be repeated for the modified models with linear elastic and also viscoelastic legs. But applying the flexibility effects of the legs even small deflection causes changes in transition rules, because these passive walkers are very sensitive to small variations in their modeling. Due to the impulsive nature of the impact forces, the robot configuration remains unchanged during the collision with the ground. Thus, the transition rule of positions of the viscoelastic legs is written as follow

$$\begin{Bmatrix} \theta_{st} \\ v_i \\ \phi \\ p_i \end{Bmatrix}^{+} = \underbrace{\begin{bmatrix} -1 & \mathbf{0} & 0 & \mathbf{0} \\ \mathbf{0}^T & I_n & \mathbf{0}^T & 0_n \\ 0 & \mathbf{0} & -1 & \mathbf{0} \\ \mathbf{0}^T & 0_n & \mathbf{0}^T & I_n \end{bmatrix}}_{\boldsymbol{J}} \begin{Bmatrix} \theta_{st} \\ v_i \\ \phi \\ p_i \end{Bmatrix}^{-} \quad , \quad i = 1, \dots, n \tag{23}$$

where I_n and 0_n are the $n \times n$ identity matrix and zero matrix, respectively; $\mathbf{0}$ is the $1 \times n$ zero vector and $\mathbf{0}^T$ represents the transpose of it.
Since the impact forces are the only external forces affecting the biped, the angular momentum of the whole mechanism and the former stance leg (new swing leg) around the impact point and the hip is conserved before and after the collision. Presented below are two expressions for the small mass elements of the viscoelastic legs that exploit the angular momentum balance to derive the update of the angular velocities as given in [37].

$$\int \vec{r}_{O^- p_{st}^-} \times \vec{v}_{st}^- \, dm_{st} + \int \vec{r}_{O^- p_{sw}^-} \times \vec{v}_{sw}^- \, dm_{sw} + M\vec{r}_{O^- C_H^-} \times \vec{v}_H^- = \int \vec{r}_{O^+ p_{st}^+} \times \vec{v}_{st}^+ \, dm_{st} + \int \vec{r}_{O^+ p_{sw}^+} \times \vec{v}_{sw}^+ \, dm_{sw} + M\vec{r}_{O^+ C_H^+} \times \vec{v}_H^+ \tag{24}$$

$$\int \vec{r}_{C_H p_{st}^-} \times \vec{v}_{st}^- \, dm_{st} = \int \vec{r}_{C_H p_{sw}^+} \times \vec{v}_{sw}^+ \, dm_{sw}$$

The above position vectors in Eq. (22) are the distances of mass elements to the mentioned centers of rotation. Given the number of unknown velocities, there is still a need for exploring two other momentum expressions that specify the role of deflection (generalized coordinates v_i and p_i) in transition rule of velocities. As stated before in [37], these novel expressions which are the time integrals of the Eq. (10-3) and Eq. (10-4) during the time instances just before and just after collision used to update the time derivatives of $\mathrm{w_{st}}(\mathrm{x_1}, \mathrm{t})$ and $\mathrm{w_{sw}}(\mathrm{x_2}, \mathrm{t})$for each leg. According to switching of the viscoelastic legs at the moment of impact, the conservation law of momentum of these expressions is defined as

$$\left(\int \; [Eq.(12)]dt \right)^- = \left(\int \; [Eq.(13)]dt \right)^+$$

$$\dot{w}_{st}^- - x_1 \dot{\theta}_{st}^- = \dot{w}_{sw}^+ - x_2 \dot{\theta}_{st}^+ + x_2 \dot{\phi}^+$$

$$\left(\int \; [Eq.(13)]dt \right)^- = \left(\int \; [Eq.(12)]dt \right)^+ \tag{25}$$

$$\dot{w}_{sw}^- - x_2 \dot{\theta}_{st}^- + x_2 \dot{\phi}^- = \dot{w}_{st}^+ - x_1 \dot{\theta}_{st}^+$$

Then, by employing the AMM and using the orthogonality of the shape functions, the Eqs. (24)-(25) can be written in the discrete form as

$$\boldsymbol{Q}^+ \begin{Bmatrix} \dot{\theta}_{st} \\ \dot{v}_i \\ \dot{\phi} \\ \dot{p}_i \end{Bmatrix}^+ = \boldsymbol{Q}^- \begin{Bmatrix} \dot{\theta}_{st} \\ \dot{v}_i \\ \dot{\phi} \\ \dot{p}_i \end{Bmatrix}^- \quad , \quad i = 1, \dots, n \tag{26}$$

to calculate the transition rule of the velocities by following relation

$$\boldsymbol{H} = (\boldsymbol{Q}^+)^{-1} \boldsymbol{Q}^- \tag{27}$$

And finally, by merging the transition rules in Eq. (23) and Eq. (27), we obtain the jump equations like so

$$\begin{Bmatrix} \theta_{st} \\ v_i \\ \phi \\ p_i \\ \dot{\theta}_{st} \\ \dot{v}_i \\ \dot{\phi} \\ \dot{p}_i \end{Bmatrix}^{+} = \underbrace{\begin{bmatrix} \boldsymbol{J} & 0_{(2n+2)} \\ 0_{(2n+2)} & \boldsymbol{H} \end{bmatrix}}_{J_s} \begin{Bmatrix} \theta_{st} \\ v_i \\ \phi \\ p_i \\ \dot{\theta}_{st} \\ \dot{v}_i \\ \dot{\phi} \\ \dot{p}_i \end{Bmatrix}^{-} \tag{28}$$

where $0_{(2n+2)}$ is the $(2n+2)\times(2n+2)$ zero matrix and also J_s is a global transition matrix. In order for these jump equations to correctly be applied when the swing foot strikes the slope, the configuration of the robot that results in an impact must be determined. This configuration corresponds to the geometric collision condition known as the impact surface or switching surface. In contrast to the rigid model, a configuration of the flexible walker that leads to impact with the slope must satisfy the following relation

$$\boldsymbol{\Gamma}(\boldsymbol{q}) = w_{st_l} sin\theta_{st} + lcos\theta_{st} - w_{sw_l}\sin(\phi - \theta_{st}) - l\cos(\phi - \theta_{st}) = 0 \tag{29}$$

The switching surface $\boldsymbol{\Gamma}$ is detected when the swing leg reaches the walking surface, while it is in front of the stance leg and is also moving downward. It is transparent that the transition rules at the impact collision are still valid by replacing the elastic legs with viscoelastic beams.

2.1.4. Hybrid dynamics

Using the continuous dynamics in Eq. (20), together with the impact surface defined by Eq. (29) and the algebraic transition rules in Eq. (28), a complete mathematical model of the walking biped can be illustrated as a diagram in Fig. 2.

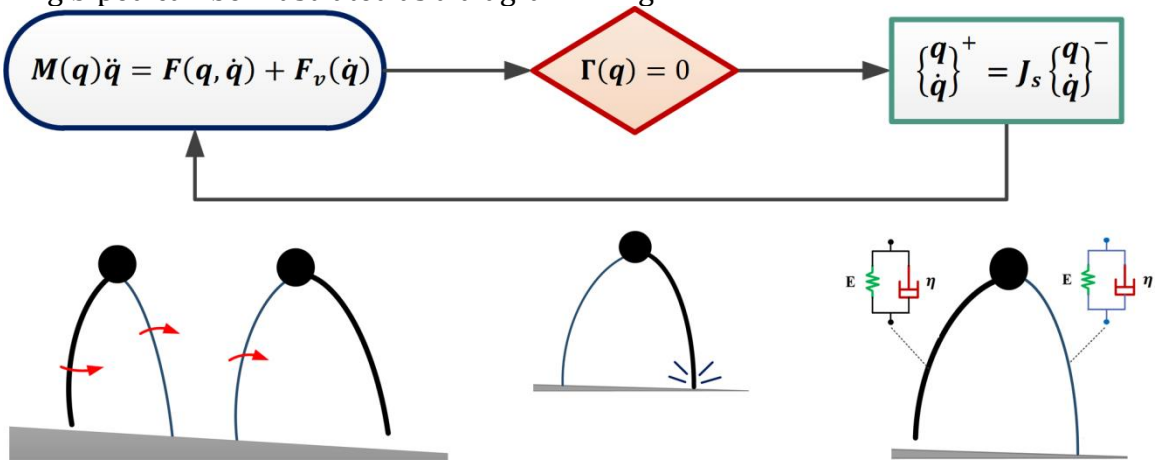

Figure 2: Hybrid dynamics of the flexible passive walker with viscoelastic legs.

2.2. Methodology for finding period-one gait cycles

In this subsection, we will focus on exploring proper initial conditions of period-one gait cycles of the simplest passive walkers with viscoelastic legs by an effective numerical method as proposed in our previous works [37,42].

Almost all the existing bipedal walkers based on passive dynamic walking start walking only through certain initial conditions; otherwise, the robot will fall down. Finding stable walking motions relies on these appropriate initial conditions which are located in a quite narrow region called the basin of attraction. Although this fractal-like shaped area limits the performance of the passive walker from the viewpoint of stability and control, this shortcoming can be remedied by offering some solutions [43,44].

Because of nominally periodic sequence of steps, an effectual tool for studying the impulsive hybrid nonlinear dynamics of walking is based on interpreting a step as a Poincaré map. This map is a stride function [45] relating the state during one part of a step with the state during the same part of the next step, reading

$$\begin{Bmatrix} \boldsymbol{q}^{+} \\ \dot{\boldsymbol{q}}^{+} \end{Bmatrix}^{i+1} = \boldsymbol{S}\left(\begin{Bmatrix} \boldsymbol{q}^{+} \\ \dot{\boldsymbol{q}}^{+} \end{Bmatrix}^{i} \right) \tag{30}$$

From a conventional choice of initial conditions, the above mapping evaluated at the Poincaré section $\boldsymbol{\Gamma}$ just after the heel-strike collision. Gait cycles are the fixed points of the linearized Poincaré map which numerically computed from a well-chosen estimate of the initial conditions through the Newton–Raphson iterative scheme. The cyclic stability of these periodic solutions is examined by evaluating the eigenvalues of this linearized map (Jacobian matrix) at the fixed points. The walking stability is preserved if all the eigenvalues of the Jacobian matrix are inside the unit circle. It is known that a general way to identify and analyze stability of fixed points is based on implicitly numerical computation of the linearized Poincaré map, but it will be a difficult task to implement this classic technique successfully for more complex models, especially with high computational cost. In order to bypass these difficulties, proposing new strategies such as shooting method [46], explicitly defined Poincaré map [25,26] and using boundary value problem [42,47] is one of the recent directions for passive bipedal research to discover unforeseen walking patterns.

Here, following our approach in [37,42], a step function (gait cycle) will be created in a numerical process based on the implicitly defined Poincaré map as the conception of a boundary value problem (BVP). This means that the continuous dynamics for a single walking step conceptually forms a BVP in which the boundary conditions correspond to the states at the beginning and end of the step. Indeed, these boundary conditions are related through transition rules at the impact. For a desired one-periodic gait, despite the existence of unanticipated walking patterns, the relevant BVP form of the nonlinear swing equations are reformulated as the following state space model with the state vector $\boldsymbol{x} = [\boldsymbol{q}\ \dot{\boldsymbol{q}}\ ]^T$ and the step period T,

$$\dot{\boldsymbol{x}}(t) = \begin{pmatrix} \dot{\boldsymbol{q}} \\ \boldsymbol{M^{-1}}(\boldsymbol{q})\boldsymbol{F}(\boldsymbol{q},\dot{\boldsymbol{q}}) \end{pmatrix}\ , \boldsymbol{x}(t=0^{+}) = [\boldsymbol{q}^{+} \quad \dot{\boldsymbol{q}}^{+}\ ]^T, \boldsymbol{x}(t=T^{-}) = [\boldsymbol{q}^{-} \quad \dot{\boldsymbol{q}}^{-}\ ]^T \tag{31}$$

where the initial conditions for a periodic motion $\boldsymbol{x}(t=0^{+}) = \boldsymbol{x}(t=T^{+})$ as well as the time period T are unknown. Applying finite difference method, one of the simplest and fastest ways to discretize high-order equations, it is feasible to convert the nonlinear

differential equations of the swing phase into algebraic equations. In fact, our linearization methodology lies in replacing the derivatives in the continuous dynamics by central finite difference approximations as below

$$\dot{\boldsymbol{q}}_{n_t+\frac{1}{2}} = \frac{\dot{\boldsymbol{q}}_{n_t+1} + \dot{\boldsymbol{q}}_{n_t}}{2} = \frac{\boldsymbol{q}_{n_t+1} - \boldsymbol{q}_{n_t}}{\Delta t} \quad , \quad \ddot{\boldsymbol{q}}_{n_t+\frac{1}{2}} = \frac{\dot{\boldsymbol{q}}_{n_t+1} - \dot{\boldsymbol{q}}_{n_t}}{\Delta t} \tag{32}$$

The solution of these difference equations for one step in the time interval $[0, T]$ is a discretized trajectory consisting of a series of the phase-space points $\boldsymbol{x}_{n_t} = \boldsymbol{x}(t_{n_t})$, which is divided into n_t equally subintervals of width $\Delta t = \frac{T}{N}$. After substituting relations of Eq. (32) in the Eq. (31) and linearizing it using the first-order Taylor approximation, a step-to-step calculation procedure can be obtained for n_t time intervals by the following system:

$$\begin{aligned} \boldsymbol{x}_1 &= \boldsymbol{f_s}(\boldsymbol{x}_{0^+}) \\ \boldsymbol{x}_2 = \boldsymbol{f_s}(\boldsymbol{x}_1) &= \boldsymbol{f_s}\big(\boldsymbol{f_s}(\boldsymbol{x}_{0^+})\big) \\ &\vdots \\ \boldsymbol{x}_{T^-} &= \underbrace{\boldsymbol{f_s}\Big(\dots \boldsymbol{f_s}\big(\boldsymbol{f_s}(\boldsymbol{x}_{0^+})\big)\Big)}_{n_t\ times} \end{aligned} \tag{33}$$

where $\boldsymbol{f_s}$ is the linearized form of the ordinary first-order differential equations in Eq. (31). Then, employing the jump relations in Eq. (28) at the end of a single walking step and adding the impact surface expression in Eq. (29) to pinpoint the exact instant of impact contact, our step function makes the following simplified impulsive hybrid dynamics of a walking step:

$$\boldsymbol{F_s} = \begin{bmatrix} \boldsymbol{x}_{T^+} - \boldsymbol{J_s}\boldsymbol{x}_{T^-} \\ \boldsymbol{\Gamma} \end{bmatrix} = \begin{bmatrix} \boldsymbol{x}_{T^+} - \boldsymbol{J_s}\left(\underbrace{\boldsymbol{f_s}\Big(\dots \boldsymbol{f_s}\big(\boldsymbol{f_s}(\boldsymbol{x}_{0^+})\big)\Big)}_{n_t\ times}\right) \\ \boldsymbol{\Gamma} \end{bmatrix} \tag{34}$$

where $t = T^-$ and $t = T^+$ refer to the time instances just before and just after impact, respectively and $\boldsymbol{x}_T = \boldsymbol{x}(t = T)$.

In a nutshell, the produced multidimensional step function contains the following aspects: 1) nonlinear algebraic equations obtained from finite difference solution (discretization) of continuous dynamics, 2) end-of-step (heel-strike) detection, and 3) transition rules. From Eq. (34), it is clear that the appropriate initial conditions $\boldsymbol{x}_{0^+}$ and the correspondent time period T are the unknown variables or the zeros of the step function. They can be numerically calculated by using the capabilities of MATLAB software in the Optimization Toolbox (root finding by *Fsolve*) if a good starting point is supplied.

Now, using the favorable initial conditions and the impulsive hybrid dynamics in the state space form, we have sufficient tools to simulate a cyclic walking motion as an Initial Value Problem (IVP) by defining the resulted $\boldsymbol{x}_0$ as initial values. The capabilities of Matlab software are employed in order to utilize the numerical differential solvers for solving ordinary differential equations (ODEs). The numerical integration of the IVP is performed using the default solver ODE45 with desired accuracy and event function is used to detect zero-crossing of certain algebraic expression in the solver, in this case it notifies when the impact surface in Eq. (29) crosses zero. When ode45 receives this notification, the

integration is stopped and the transitions rules in Eq. (28) are applied to calculate the updated positions and velocities of the biped. Hence, as this trend continues, the period-one gait cycle of the flexible passive walker can be simulated.
It is worth to mention that the presented method provides two features: quick calculation and easy implementation in particular for complicated passive models like this flexible biped robot.

3. Simulation results and discussion

This section will show, through theoretical simulation results, the efficiency of the assumed viscoelastic legs for the simplest passive biped robot. In the first set of simulations, proper initial conditions and then period-one gait cycles are determined by using the suggested method for a flexible passive walker with the default parameter values. Note that the structural parameters of the simplest passive walker can be freely defined, since the biped robot under study in this paper is not based on a physical machine. However, for comparison purposes, the parameters assigned to the walker are similar to those found in [3,37] and are given in Table 1. Also, we will use just one flexible mode for each leg i.e. $n = 1$. The next sets of simulations are obtained using the bifurcation diagrams, which demonstrate the effects of the slope angle and the dimensionless mass on the dynamic behavior of the flexible models in Table 1 compared to each other.

Table 1: Structural parameters and initial conditions for gait patterns of the flexible models.

Models	**Damping coefficients**	**Initial conditions** $[\theta_{st_0}, v_0, \phi_0, p_0\ ], [\dot{\theta}_{st_0}, \dot{v}_0, \dot{\phi}_0, \dot{p}_0]$	**Structural parameters**
Pure elastic	$\bar{\eta} = 0$	$[0.0917, 27.38 \times 10^{-6}, 0.1835, -46.68 \times 10^{-7}]$ $[-0.1079, 0.00468, -0.0016, -0.00504]$	$\gamma = 0.001\ (rad)$ $D = 10^3$ $\bar{M} = 50$ $L = 1\ m$ $g = 10\ m/s^2$ $\rho A = 1\ kg/m$ $I = 0.05 \times 10^{-5}\ m^4$
Damped elastic (The linear viscous)	$\zeta = 0.05$	$[0.0956, 2.06 \times 10^{-7}, 0.1913, 1.07 \times 10^{-7}]$ $[-0.0996, -1.115 \times 10^{-7}, -0.0036, 2.16 \times 10^{-7}]$	
Viscoelastic	$\bar{\eta} = 0.001$	$[0.0956, 2.06 \times 10^{-7}, 0.1913, 1.07 \times 10^{-7}]$	

(The Kelvin-Voigt model)	$[-0.0996, -1.115 \times 10^{-7}, -0.0036, 2.16 \times 10^{-7}]$	

3.1. Typical walking gait

Before any gait cycle can be analyzed, first the nonlinear algebraic equations defined as a step function in Eq. (34) must be solved iteratively, whose converged solutions depend upon the initial guess. It is important to note that a reasonable choice of this starting guess, meaning within the neighborhood of the desired initial conditions, can provide a suitable solution. In this way, the exact initial conditions resulted for the simplest passive walker with pure elastic legs in our previous work [37] (as seen in Table 1) are used as the initial guess of the step function (*Fsolve* function in Matlab) of the walker with viscoelastic legs. After this stage, it is time to find walking patterns numerically by application of the IVP (using ODE45 in Matlab) as described in subsection 2.2 and started with the proper initial conditions from Table 1. Fig. 3 and Fig. 4 show these simulation results including the period-one gait cycle, the time evolution of angular velocities and the variations of the time-dependent generalized coordinates of the flexible walker with viscoelastic legs. We noted previously in [37] that non-periodic gait cycle was found for the elastic legs with unwanted vibrations. But it is evident from Fig. 3 that using viscoelastic material significantly reduces the vibrations of pure elastic legs and the period-one symmetric steady gait cycle can be obtained. Looking at Fig. 4, it is clear that the flexural deflections of the viscoelastic legs are not symmetric during walking pattern. In fact, the resulted symmetric gaits arise here from asymmetric viscoelastic legs with different deformations. Notice that although the passive walking pattern is simulated for small transverse displacements, we can not ignore the influence of small deflections on the impulsive hybrid dynamics of the flexible walker, as seen in [37].

The phase portrait diagram and the loci of the eigenvalues of the Jacobian matrix of the step function are also plotted in Fig. 5. The local stability of the closed orbit in Fig. 5(a) can be analyzed by checking the eigenvalues of the Jacobian at the obtained fixed point. As anticipated, all of the eigenvalues are in the unit circle as seen in Fig. 5(b) and thus this phase portrait shows convergence to the stable limit cycle of the passive biped robot with viscoelastic legs. Recall that the corresponding Jacobian matrix is calculated by simulating one step for a small perturbation on each of the states of the fixed point.

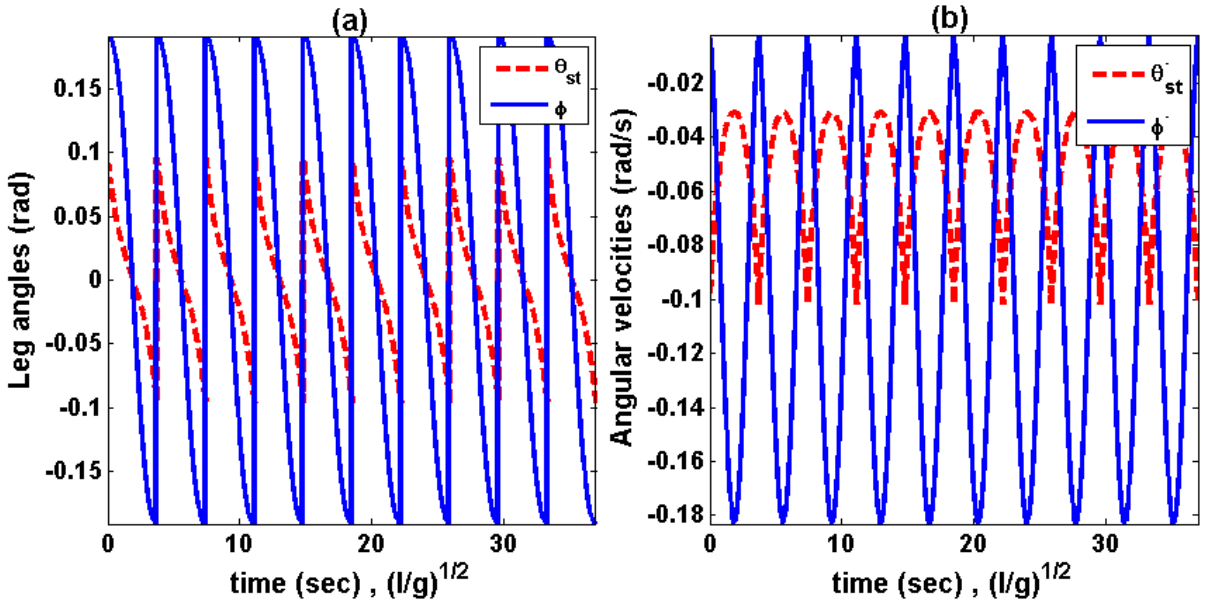

Figure 3: (a) Leg angles (b) angular velocities versus time through a stable gait cycle of the flexible simplest passive walker with viscoelastic legs for 10 first steps ($\bar{\eta} = \mathbf{0.001}, \boldsymbol{D} = \mathbf{10^3}, \boldsymbol{\gamma} = \mathbf{0.001}\ \boldsymbol{rad}$).

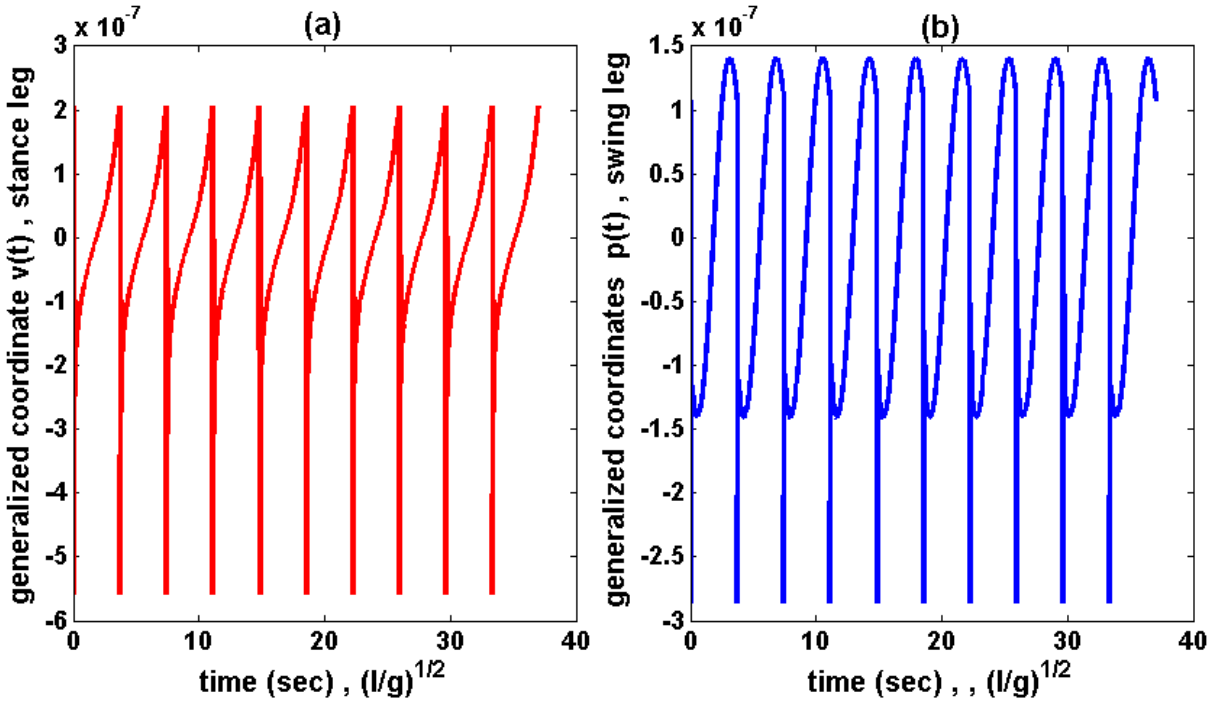

Figure 4: Variations of the generalized coordinates through a stable gait cycle of the flexible simplest passive walker with viscoelastic legs for 10 first steps ($\bar{\eta} = \mathbf{0.001}, \boldsymbol{D} = \mathbf{10^3}, \boldsymbol{\gamma} = \mathbf{0.001}\ \boldsymbol{rad}$).

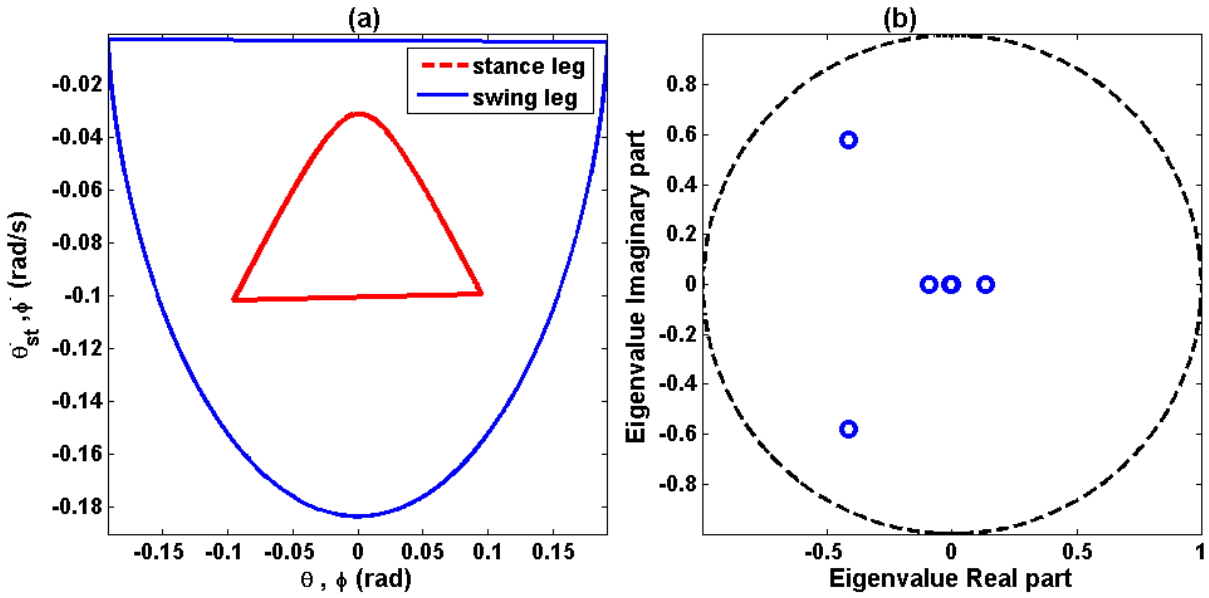

Figure 5: (a) Phase portrait diagram (b) Loci of eigenvalues for a stable gait cycle of the flexible simplest passive walker with viscoelastic legs ($\boldsymbol{\eta^{-} = 0.001}$, $\boldsymbol{D = 10^3}$, $\boldsymbol{\gamma = 0.001\ rad}$).

As explained in [37], we used proportional damping (in the form of Rayleigh damping) to damp the vibrations of the pure elastic legs regardless of its limitations. The results showed that by increasing the damping ratio, the vibrations completely damp out and the flexible biped robot behaves almost like corresponding rigid passive walker for the same slope angle. The obtained initial conditions for a sample of these damped elastic legs with high damping ratio are given in Table 1. Fig. 6 reveals the variations of the leg angles for the flexible cases in Table 1 compared to the similar rigid model. As seen, for the first few steps, the leg angles of the flexible models with damping technology are fairly close to the rigid model and the differences grow as time goes on. Nevertheless, the proportional damping model requires high damping ratio for the same performance compared to the viscoelastic material. Our further investigation demonstrates that assuming low damping coefficient ($\bar{\eta} < 0.001$) leads to non-periodic gait cycles for the walker with viscoelastic leg. This result is quite obvious, so we refuse to present the corresponding figure. Even in this case, as clearly depicted in Fig. 7, the viscoelastic leg provides a better robustness against vibrations than the similar elastic leg with low damping ratio ($\zeta = 10^{-4}$) and finally the angular velocities of both flexible legs will be shown fewer oscillations.

Besides the practical limitation of a simple viscous damping (proportional damping), in some special applications such as artificial muscles, the intrinsic viscosity of the structure is the dominant property of the system. Therefore, we are interested in the use of commercially available viscoelastic materials for the compliant legs and also gain insight into the application of passive dynamic walking in building an efficient biped robot.

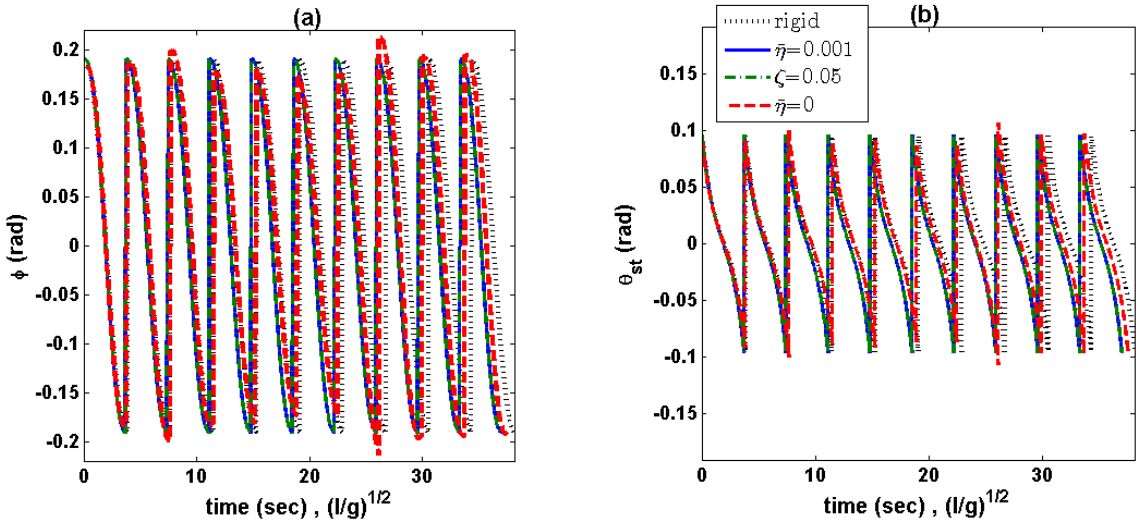

Figure 6: Variations of the leg angles for different legs of the flexible simplest passive walker according to Table 1 compared to the rigid model ($\bar{M} = 50$, $D = 10^3$, $\gamma = 0.001\ rad$).

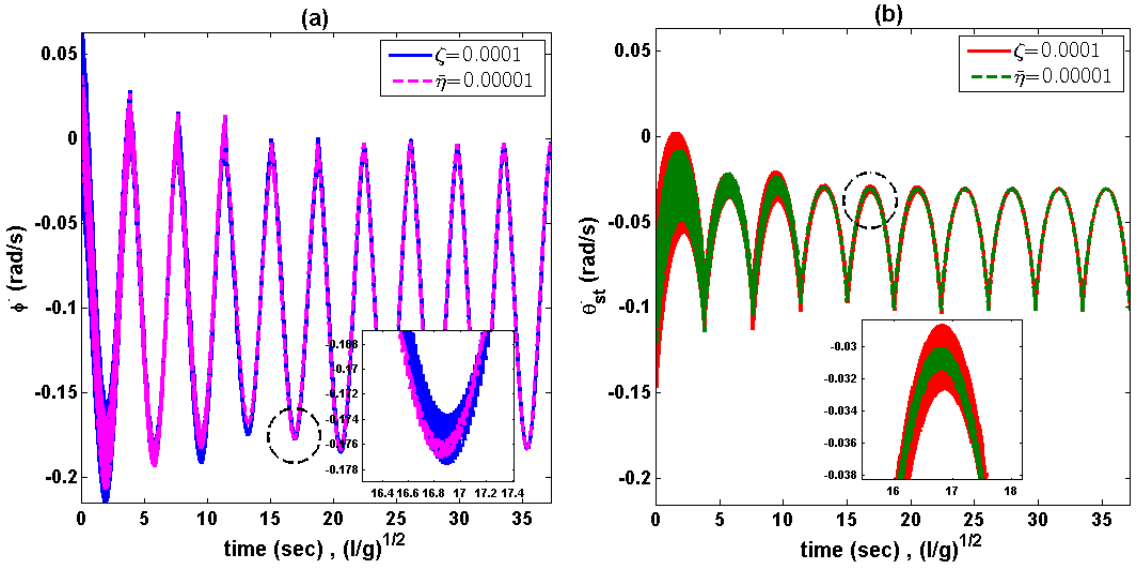

Figure 7: Variations of the oscillations in the angular velocities of the viscoelastic legs and the low damped elastic legs ($\bar{M} = 50$, $D = 10^3$, $\gamma = 0.001\ rad$).

3.2. Parameter study

This part is devoted to examine the effectiveness of the essential parameters: the ground slope γ and the dimensionless mass $\bar{M}$ on the walking motion. By varying these two parameters in the dynamic equations of passive walking, the bifurcation diagrams of the models with viscoelastic and high damped elastic legs as well as the corresponding rigid

model can be drawn for certain other parameter values in Table 1. In the present investigation, the bifurcations are observed from the stance leg angle, the angular velocities of both legs and the step period. Although the concept of bifurcation and chaos for the passive biped robots is a vast field of study, we focused on the variations in the region of period-one gaits.

As seen in Garcia's study [3,4], changes in the slope angle give rise to period doubling bifurcations leading to chaos. Our numerical simulations in Figs. 8-11 for the simplest passive walking with two identical viscoelastic, high damped elastic and rigid legs also display this scenario. These figures represent the comparison between the models from the occurrence of the first period-doubling bifurcation and also the region of existing period-one stable gaits. According to these simulation results, using flexible legs decreases the highest slope for stable period-one gaits from 0.0121 (of the rigid model) to $\gamma < 0.0625$. In contrast, both flexible models exhibit the same walking characteristics and there is not much difference between their maximum reachable slope angles for period-one motions because of the high damping ratio of the elastic legs. In other words, the damped elastic legs will be as efficient as the viscoelastic legs if high damping ratio is considered. Generally, it appears that assuming viscoelastic legs expands the region of period-one gait cycles compared to the damped elastic model.

In a similar manner with the high damped elastic legs [37], the displayed bifurcation diagram in Fig. 8 confirms that the flexible model with viscoelastic legs follows the walking pattern of the basic rigid model on shallow slope angles. The results in Fig.9 and Fig. 10 show that the angular velocity of the stance viscoelastic leg generates the same behavior as that obtained by means of the rigid stance leg, whereas the angular velocity of the swing viscoelastic leg has such a large difference with the rigid swing leg. Apart from that, the angular velocities of both viscoelastic legs decrease as the slope increases. From Fig. 11, it can be seen that the inclination angle has a small influence on the step period of all models. Moreover, the steps of the passive walker with viscoelastic legs are shorter and faster than the rigid biped.

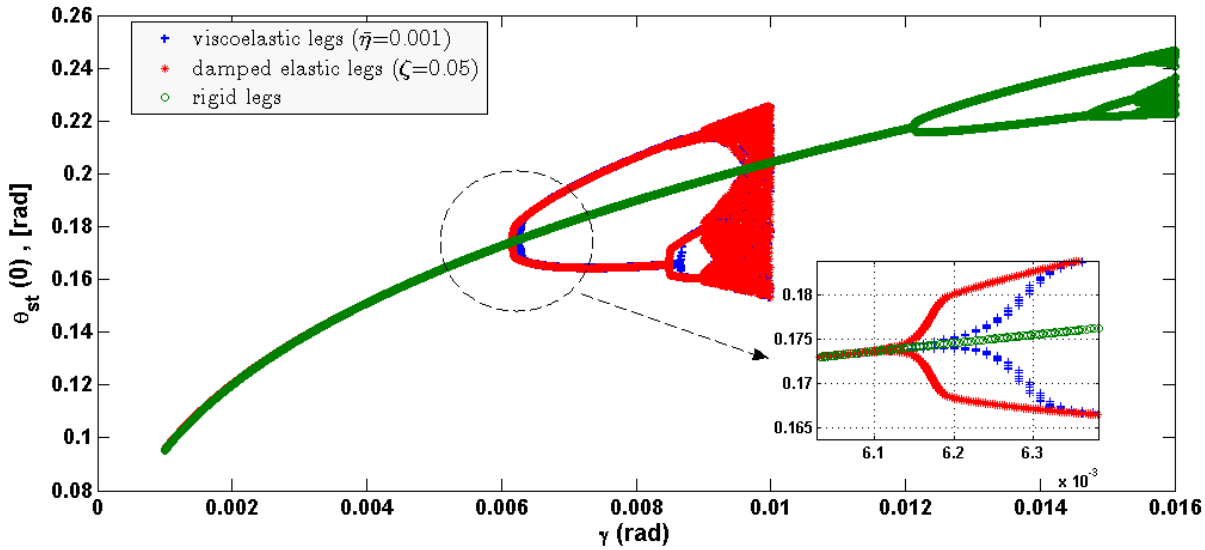

Figure 8: Variations of $\boldsymbol{\theta(0)}$ as a function of the slope angle for the rigid and flexible simplest walking models ($\bar{\boldsymbol{M}} = \mathbf{50}\,, \boldsymbol{D} = \mathbf{10^3}$).

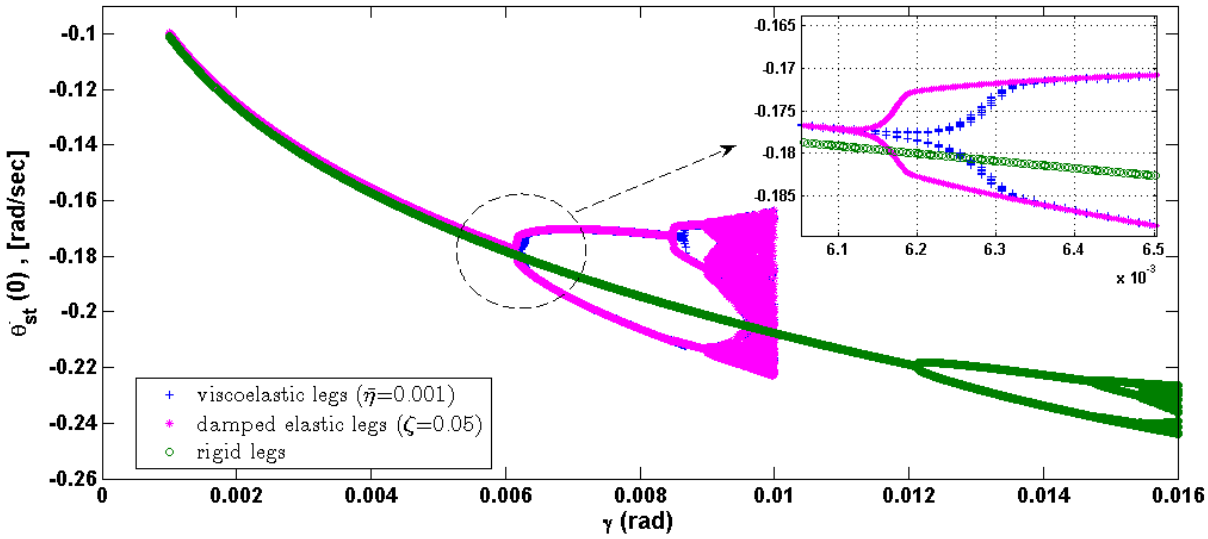

Figure 9: Variations of $\dot{\boldsymbol{\theta}}(\mathbf{0})$ as a function of the slope angle for the rigid and flexible simplest walking models ($\bar{\boldsymbol{M}} = \mathbf{50}\,, \boldsymbol{D} = \mathbf{10^3}$).

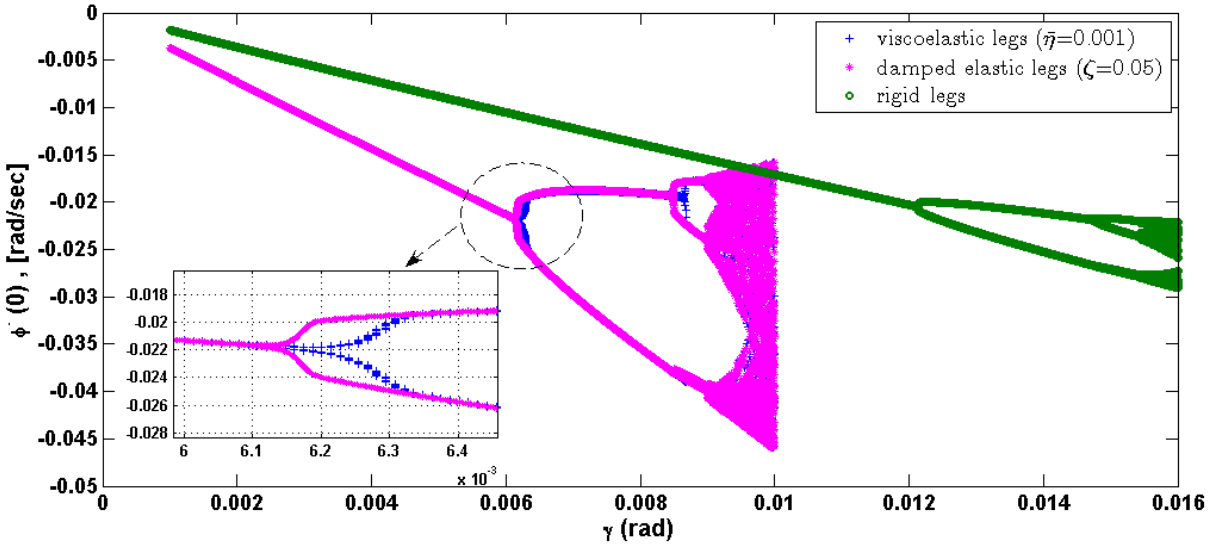

Figure 10: Variations of $\dot{\boldsymbol{\phi}}(\mathbf{0})$ as a function of the slope angle for the rigid and flexible simplest walking models ($\bar{\boldsymbol{M}} = \mathbf{50}\,, \boldsymbol{D} = \mathbf{10^3}$).

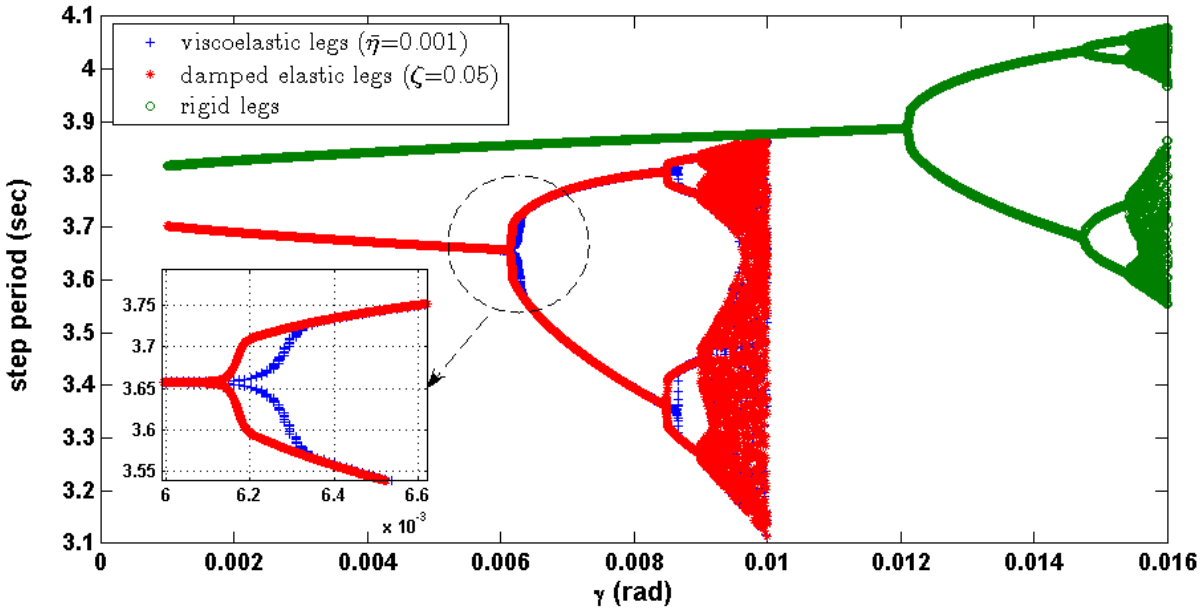

Figure 11: Variations of the step period as a function of the slope angle for the rigid and flexible simplest walking models ($\bar{\boldsymbol{M}} = \mathbf{50}$, $\boldsymbol{D} = \mathbf{10^3}$).

In the sequel, we investigate the effect of mass ratio $\bar{M}$ through the bifurcation diagrams in Fig. 12 and Fig. 13. As depicted, by increasing the mass ratio, the walking pattern and its properties remain almost constant, but the first bifurcation point is shifted backward along with the increase in slope angle. The main cause of this remarkable change is increasing the leg deflection at the steeper slopes. Despite these identical results for both viscoelastic and elastic legs with high damping ratio, using viscoelastic material is still lead to the development of the stable period-one region.

In an effort to improve the accuracy of the assumed modes discretization method, the number of mode shapes used in the viscoelastic model (as defined in Table. 1) increases and henceforth we computed the bifurcation diagrams for two assumed mode shapes ($n = 2$). The graphs in Fig. 14, Fig. 15 and Fig. 16 illustrate that by applying the higher mode shapes, the style of walking is preserved and only the first bifurcation point is slightly shifted forward as the slope angle varies. Apparently, this approximate increase of the stable period-one region is even beneficial to the walking stability, in contrast with the other studied flexible passive models in Table. 1.

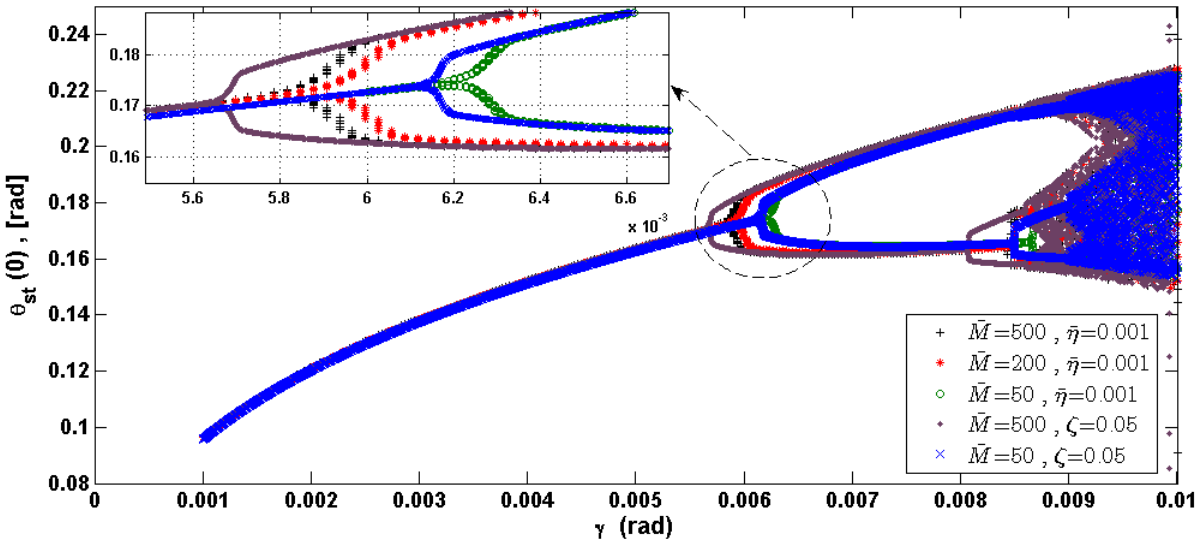

Figure 12: Variations of the stance leg angle of the flexible simplest walking models as a function of the slope for different magnitudes of $\bar{M}$ ($D = 10^3$).

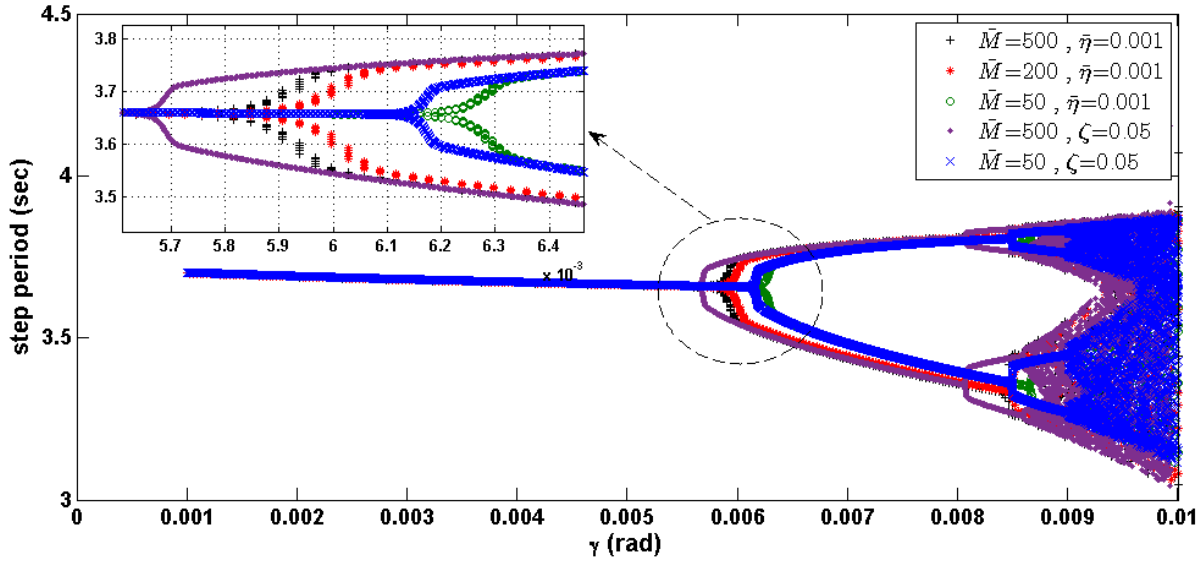

Figure 13: Variations of the step period of the flexible simplest walking models as a function of the slope for different magnitudes of $\bar{M}$ ($D = 10^3$).

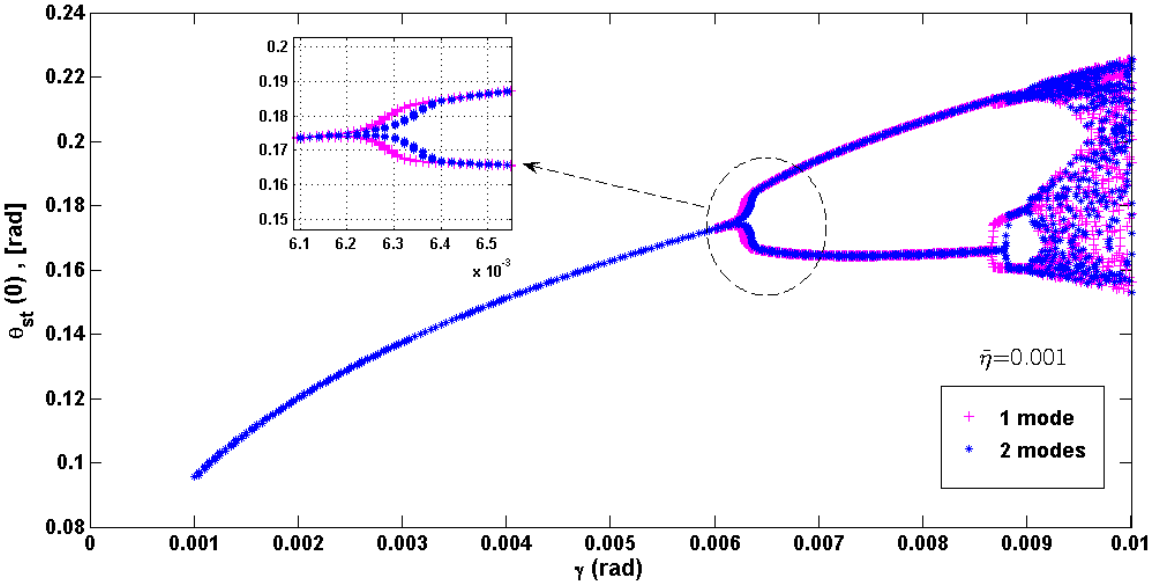

Figure 14: Variations of $\boldsymbol{\theta(0)}$ of the flexible simplest walking model with viscoelastic legs as a function of the slope for different mode shapes ($\bar{\eta} = 0.001, D = 10^3, \bar{M} = 50$).

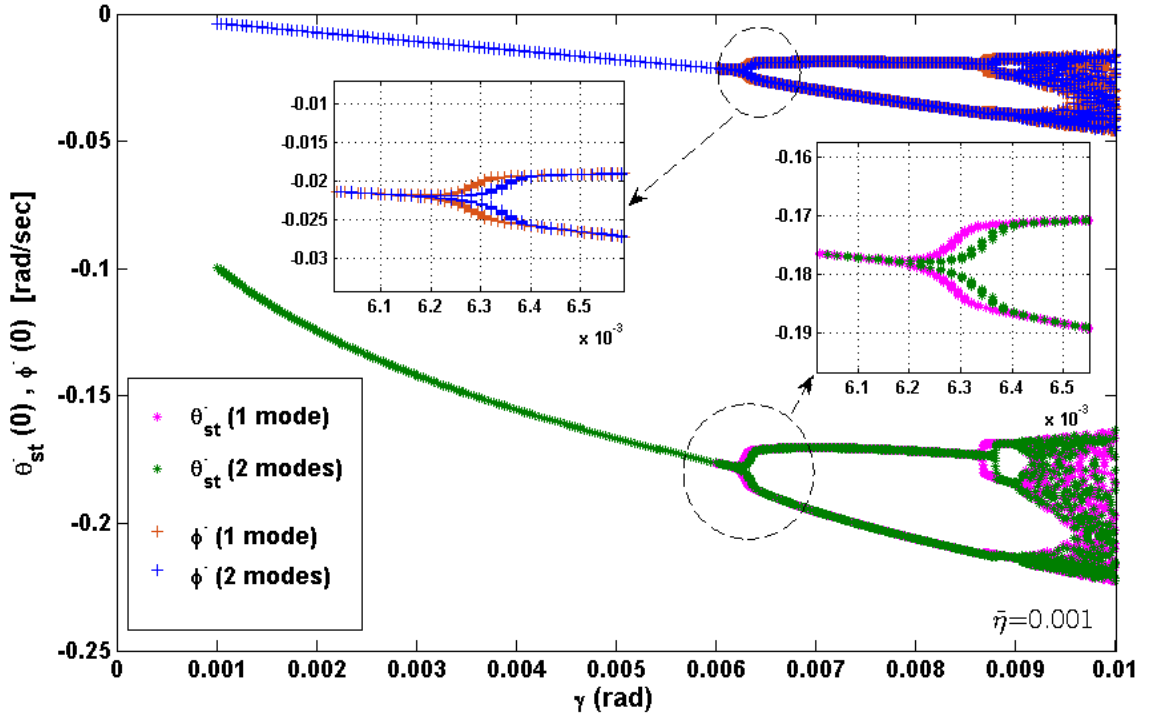

Figure 15: Variations of $\dot{\boldsymbol{\theta}}(\mathbf{0})$ and $\dot{\boldsymbol{\phi}}(\mathbf{0})$ of the flexible simplest walking model with viscoelastic legs as a function of the slope for different mode shapes ($\bar{\eta} = 0.001, D = 10^3, \bar{M} = 50$).

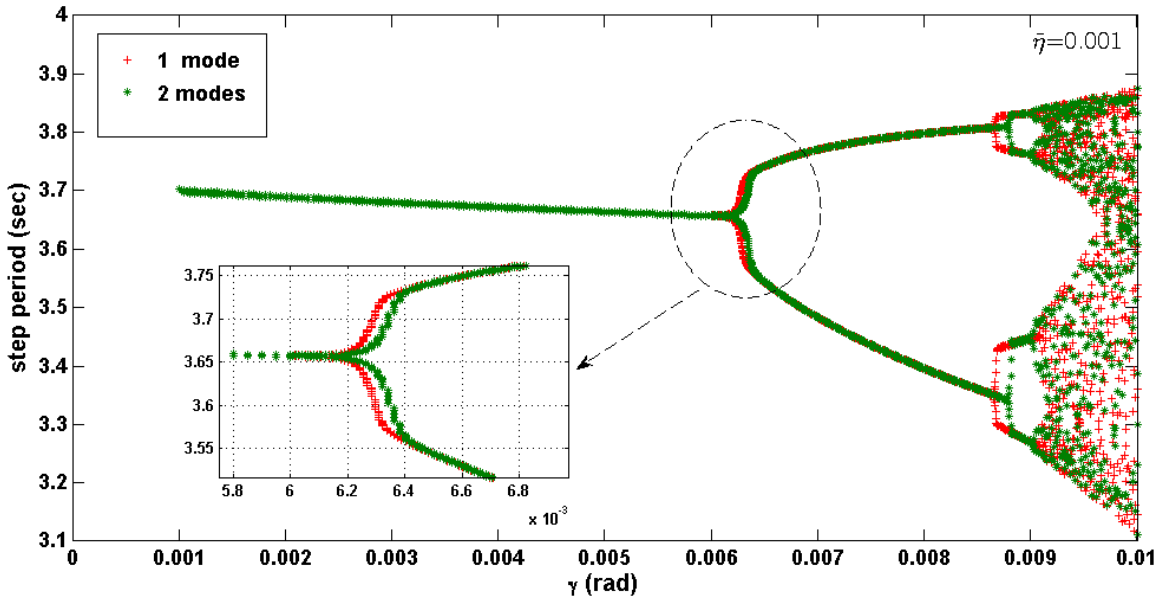

Figure 16: Variations of the step period of the flexible simplest walking model with viscoelastic legs as a function of the slope for different mode shapes ($\bar{\eta} = 0.001, D = 10^3, \bar{M} = 50$).

4. Conclusions

In this paper, a further study on the simplest passive biped robot, with a high modeling accuracy, using the structural viscoelasticity (Kelvin–Voigt) effect as a damping mechanism of the flexible leg has been presented. The updated mathematical model of the walking motion that described by an impulsive hybrid nonlinear dynamics including nonlinear differential equations and a nonlinear algebraic equation has been obtained by the combined Lagrangian-Assumed Modes Method with specific precise boundary conditions. The main focus has been set on finding the proper initial conditions for stable period-one gait cycles that are the fixed points of the new constructed step function and then simulating the walking pattern as an IVP by defining the resulted stable initial conditions as initial values.

By employing the proposed approach, via numerical simulations, we have showed the period-one gait cycle for the simplest passive walker with the Kelvin–Voigt viscoelastic legs. Moreover, the effects of the system parameters containing the mass ratio and the slope angle have been investigated through bifurcation diagrams. Regarding the material properties of the flexible legs (viscoelastic vs. elastic), it was concluded that the viscoelastic legs increased the stability of the model on shallow slopes, even with high mass ratio or two mode shapes compared to the high damped elastic legs. These results convincingly confirm the important role of the viscoelastic leg as an energy dissipater in the flexible passive walker.

Conflict of Interest:

The authors declare that they have no conflict of interest.

Funding:

No funding was received for this work.

Appendix A. Definition of the normalized matrices of the flexible model with viscoelastic legs

In this appendix, we derive the upper triangular elements of the symmetric inertia matrix and the right hand side vector in Eq. (20) for the first mode shape ($n = 1$) as following:

$$\begin{bmatrix} M_{11} & M_{12} & M_{13} & M_{14} \\ \dots & M_{22} & M_{23} & M_{24} \\ \dots & \dots & M_{33} & M_{34} \\ & & \dots & M_{44} \end{bmatrix} \begin{Bmatrix} \ddot{\theta} \\ \ddot{v}_1 \\ \ddot{\phi} \\ \ddot{p}_1 \end{Bmatrix} = \begin{Bmatrix} F_1(\boldsymbol{q}, \dot{\boldsymbol{q}}) \\ F_2(\boldsymbol{q}, \dot{\boldsymbol{q}}) \\ F_3(\boldsymbol{q}, \dot{\boldsymbol{q}}) \\ F_4(\boldsymbol{q}, \dot{\boldsymbol{q}}) \end{Bmatrix} + \begin{Bmatrix} F_{v_1}(\dot{\boldsymbol{q}}) \\ F_{v_2}(\dot{\boldsymbol{q}}) \\ F_{v_3}(\dot{\boldsymbol{q}}) \\ F_{v_4}(\dot{\boldsymbol{q}}) \end{Bmatrix}$$

$$M_{11} = \frac{5}{3} + \bar{v}_1^2(\tau)\left(\int_0^1 \varphi_1^2(\bar{x}_1)\, d\bar{x}_1 + \varphi_1^2(1)\right) + \bar{p}_1^2(\tau)\int_0^1 \psi_1^2(\bar{x}_2)\, d\bar{x}_2 + m_H\left(1 + \bar{v}_1^2(\tau)\varphi_1^2(1)\right)$$

$$M_{12} = -\left(\int_0^1 \bar{x}_1\, \varphi_1(\bar{x}_1) d\bar{x}_1 + (1 + m_H)\varphi_1(1)\right)$$

$$M_{13} = -\left(\frac{1}{3} + \bar{p}_1^2(\tau)\int_0^1 \psi_1^2(\bar{x}_2)\, d\bar{x}_2\right) \quad , \quad M_{14} = -\int_0^1 \bar{x}_2 \psi_1(\bar{x}_2) d\bar{x}_2$$

$$M_{22} = \left(\int_0^1 \varphi_1^2(\bar{x}_1)\, d\bar{x}_1 + (1 + m_H)\varphi_1^2(1)\right)$$

$$M_{23} = 0 \quad , \quad M_{24} = 0$$

$$M_{33} = \left(\frac{1}{3} + \bar{p}_1^2(\tau)\int_0^1 \psi_1^2(\bar{x}_2)\, d\bar{x}_2\right) \quad , \quad M_{34} = \int_0^1 \bar{x}_2 \psi_1(\bar{x}_2)\, d\bar{x}_2$$

$$M_{44} = \int_0^1 \psi_1^2(\bar{x}_2)\, d\bar{x}_2$$

$$F_1(\boldsymbol{q}, \dot{\boldsymbol{q}}) = -2\dot{\bar{\theta}}_{st}\left[\bar{v}_1(\tau)\dot{\bar{v}}_1(\tau)\int_0^1 \varphi_1^2(\bar{x}_1)\, d\bar{x}_1 + (1 + m_H)\bar{v}_1(\tau)\dot{\bar{v}}_1(\tau)\varphi_1^2(1) + \bar{p}_1(\tau)\dot{\bar{p}}_1(\tau)\int_0^1 \psi_1^2(\bar{x}_2)\, d\bar{x}_2\right] + 2\dot{\bar{\phi}}\left[\bar{p}_1(\tau)\dot{\bar{p}}_1(\tau)\int_0^1 \psi_1^2(\bar{x}_2)\, d\bar{x}_2\right] - \cos(\bar{\theta}_{st}(\tau) - \gamma)\, \bar{v}_1(\tau)\left[\int_0^1 \varphi_1(\bar{x}_1)\, d\bar{x}_1 + (1 + m_H)\varphi_1(1)\right] + \cos(\bar{\theta}_{st}(\tau) - \bar{\phi}(\tau) - \gamma)\, \bar{p}_1(\tau)\int_0^1 \psi_1(\bar{x}_2)\, d\bar{x}_2 + \left(\frac{3}{2} + m_H\right)\sin(\bar{\theta}_{st}(\tau) - \gamma) - \frac{1}{2}sin(\bar{\theta}_{st}(\tau) - \bar{\phi}(\tau) - \gamma)$$

$$F_2(\boldsymbol{q}, \dot{\boldsymbol{q}}) = \bar{v}_1(\tau)\left(\int_0^1 \varphi_1^2(\bar{x}_1)\, d\bar{x}_1 + (1 + m_H)\varphi_1^2(1)\right)\dot{\bar{\theta}}_{st}^2 - \sin(\bar{\theta}_{st}(\tau) - \gamma)\left(\int_0^1 \varphi_1(\bar{x}_1)\, d\bar{x}_1 + (1 + m_H)\varphi_1(1)\right) - D\bar{v}_1(\tau)\int_0^1 \varphi_1''^2(\bar{x}_1)\, d\bar{x}_1$$

$$F_3(\boldsymbol{q},\dot{\boldsymbol{q}}) = 2\left(\dot{\bar{\theta}}_{st} - \dot{\bar{\phi}}\right)\bar{p}_1(\tau)\dot{\bar{p}}_1(\tau)\int_0^1 \psi_1^2(\bar{x}_2)\,d\bar{x}_2 - \cos(\bar{\theta}_{st}(\tau) - \bar{\phi}(\tau) - \gamma)\,\bar{p}_1(\tau)\int_0^1 \psi_1(\bar{x}_2)\,d\bar{x}_2 + \frac{1}{2}sin(\bar{\theta}_{st}(\tau) - \bar{\phi}(\tau) - \gamma)$$

$$F_4(\boldsymbol{q},\dot{\boldsymbol{q}}) = \left(\dot{\bar{\theta}}_{st} - \dot{\bar{\phi}}\right)^2 \bar{p}_1(\tau)\int_0^1 \psi_1^2(\bar{x}_2)\,d\bar{x}_2 + sin(\bar{\theta}_{st}(\tau) - \bar{\phi}(\tau) - \gamma)\int_0^1 \bar{\psi}_1(\bar{x}_2)\,d\bar{x}_2 - D\bar{p}_1(\tau)\int_0^1 \psi_1''^2(\bar{x}_2)\,d\bar{x}_2$$

$$F_{v_1}(\dot{\boldsymbol{q}}) = 0 \quad , \quad F_{v_2}(\dot{\boldsymbol{q}}) = -\bar{\eta}D\dot{\bar{v}}_1(\tau)\int_0^1 \varphi_1''''(\bar{x}_1)d\bar{x}_1$$

$$F_{v_3}(\dot{\boldsymbol{q}}) = 0 \quad , \quad F_{v_4}(\dot{\boldsymbol{q}}) = -\bar{\eta}D\dot{\bar{p}}_1(\tau)\int_0^1 \psi_1''''(\bar{x}_2)d\bar{x}_2$$

To see the matrices Q^+ and Q^- in the jump equations, the readers are referred to our former study in [37].

$$Q^+\begin{Bmatrix}\theta_{st}\\ v_1\\ \phi\\ p_1\end{Bmatrix}^+ = Q^-\begin{Bmatrix}\theta_{st}\\ v_1\\ \phi\\ p_1\end{Bmatrix}^-$$

References

[1] T. McGeer, Passive dynamic walking, Int. J. Robot. Res. 9 (2) (1990) 62–68.

[2] A. Goswami, B. Thuilot, B. Espiau, Compass-like biped robot. Part I: Stability and bifurcation of passive gaits, INRIA. Technical Report. 2996 (1996).

[3] M. Garcia, A. Chatterjee, A. Ruina, M. Coleman, The simplest walking model: stability, complexity and scaling, J. Biomech. Eng. 120 (2) (1998) 281–288.

[4] M. Garcia, A. Chatterjee, A. Ruina, Efficiency speed and scaling of two-dimensional passive-dynamic walking, Int. J. Dyn. Stab. Syst. 15 (2000) 75–99.

[5] A. Goswami, B. Espiau, A. Keramane, Limit cycles and their stability in a passive bipedal gait, Proc. of the IEEE conference on robotics and automation, 1996. pp. 246–51.

[6] A. Goswami, B. Thuilot, B. Espiau, A study of the passive gait of a compass-like biped robot: symmetry and chaos, Int. J. Robot. Res. 17 (12) (1998) 1282–1301.

[7] K. An, Q. Chen, A passive dynamic walking model based on knee-bend behaviour: stability and adaptability for walking down steep slopes, Int. J. Adv. Robot. Syst. 10 (365) (2013) 1–11.

[8] M. Wisse, A.L. Schwab, F.C.T. Vander Helm, Passive dynamic walking model with upper body, Robotica 22 (6) (2004) 681–688.

[9] M. Kwan, M. Hubbard, Optimal foot shape for a passive dynamic biped, J. Theor. Biol. 248 (2) (2007) 331–339.

[10] Y. Jeon, YS. Park, Youngjin. Park, A study on stability of limit cycle walking model with feet: Parameter study, Int. J. Robot. Syst. 10 (1) (2013).

[11] H. Sadeghian, M. Barkhordari, Orbital analysis of passive dynamic bipeds; the effect of model parameters and stabilizing arm, J. Mech. Sci. 178 (2020).

[12] A. T.Safa, M.G. Saadat, M. Naraghi, Passive dynamic of the simplest walking model:Replacing ramps with stairs, Mech. Mach. Theory. 42 (10) (2007) 1314-1325.

[13] E. Corral, M.J. Gómez, C. Castejon, J. Meneses, R. Gismeros, Dynamic Modeling of the Dissipative Contact and Friction Forces of a Passive Biped-Walking Robot, Appl. Sci. 10 (7) (2020) 2342.
[14] H. Gritli , N. Khraief, S. Belghith, Chaos control in passive walking dynamics of a compassgait model, Commun. Nonlinear Sci. Numer. Simul. 18 (8) (2013) 2048–2065.
[15] D. Renjewski, A. Spröwitz, A. Peekema, M. Jones, J. Hurst, Exciting engineered passive dynamics in a bipedal robot, IEEE Transactions on Robotics 31 (5) (2015) 1244–1251.
[16] A. T.Safa, M. Naraghi, The role of walking surface in enhancing the stability of the simplest passive dynamic biped, Robotica 33 (1) (2015) 195–207.
[17] H. Gritli , N. Khraeif , S. Belghith , OGY-based control of chaos in semi–passive dynamic walking of a torso-driven biped robot, Nonlinear Dyn. 79 (2) (2015) 1363–1384.
[18] A. T.Safa, S. Mohammadi, S. E. Hajmiri, M. Naraghi, A. Alasty, How local slopes stabilize passive bipedal locomotion?, Mech. Mach. Theory. 100 (2016) 63-82.
[19] H. Gritli, S. Belghith, Walking dynamics of the passive compass-gait model under OGY-based control: emergence of bifurcations and chaos, Commun Nonlinear Sci Numer Simul 47 (2017) 308–327.
[20] H. Gritli, S. Belghith, Walking dynamics of the passive compass-gait model under OGY-based state-feedback control: Analysis of local bifurcations via the hybrid poincaré map, Chaos, Solitons & Fractals 98 (2017) 72 – 87.
[21] H. Razavi, A.M. Bloch, C. Chevallereau, J. W. Grizzle, Symmetry in legged locomotion: a new method for designing stable periodic gaits, Auton Robots, 41 (5) (2017) 1119–1142.
[22] H. Gritli, S. Belghith, Diversity in the nonlinear dynamic behavior of a one degree-of-freedom impact mechanical oscillator under OGY-based state-feedback control law: Order, chaos and exhibition of the border-collision bifurcation, Mech. Mach. Theory. 124 (2018) 1–41.
[23] H. Gritli, S. Belghith, Walking dynamics of the passive compass-gait model under OGY-based state-feedback control:Rise of the Neimark–Sacker bifurcation, Chaos, Solitons and Fractals, 110 (2018) 158–168.
[24] SM. Moghadam, MS. Talarposhti, A. Niaty, F. Towhidkhah, S. Jafari, The simple chaotic model of passive dynamic walking, Nonlinear Dyn, 93 (3) (2018) 1183-99.
[25] W. Znegui , H. Gritli , S. Belghith , Stabilization of the passive walking dynamics of the compass-gait biped robot by developing the analytical expression of the controlled Poincarémap, Nonlinear Dyn. 101 (2020) 1061–1091.
[26] W. Znegui, H. Gritli, S. Belghith, Design of an explicit expression of the Poincarémap for the passive dynamic walking of the compass-gait biped model, Chaos, Solitons and Fractals 130 (2020) 109436.
[27] S. Iqbal, X.Z. Zang, Y.H. Zhu, J. Zhao, Bifurcations and chaos in passive dynamic walking: A review, Robot. Auton. Syst. 62 (6) (2014) 889–909.
[28] S. Gupta, A. Kumar, A brief review of dynamics and control of under-actuated biped robots, Int. J. Adv. Robot. Syst. 31 (12) (2017) 607–623.
[29] Z. Li, NG. Tsagarakis, DG. Caldwell, Walking pattern generation for a humanoid robot with compliant joints, (2013) 1-14.
[30] Q. Wang, Y. Huang, L. Wang, Passive dynamic walking with flat feet and ankle compliance, Robotica 28 (3) (2010) 413-425.

[31] Narukawa, Terumasa, M. Takahashi, K. Yoshida, Efficient walking with optimization for a planar biped walker with a torso by hip actuators and springs, Robotica 29 (4) (2011) 641-648.
[32] D. Kerimo ˘glu , Ö. Morgül , U. Saranli ,Stability and control of planar compass gait walking with series-elastic ankle actuation, Trans. Inst. Measur. Control 39 (3) (2017) 312–323.
[33] K. Deng , M. Zhao , W. Xu ,Passive dynamic walking with a torso coupled via torsional springs, Int. J. Humanoid Rob. 14 (01) (2017) 1650024- 1: 1650024- 12.
[34] Y. Wu , D. Yao , X. Xiao , Optimal design for flexible passive biped walker based on chaotic particle swarm optimization, J. Electr. Eng. Technol. 13 (6) (2018) 2493–2503.
[35] M. Fathizadeh , H. Mohammadi , S. Taghvaei , A modified passive walking biped model with two feasible switching patterns of motion to resemble multi-pattern human walking, Chaos Solit. Fract. 127 (2019) 83–95.
[36] Y. Shen , Y. Kuang , Transient contact-impact behavior for passive walking of compliant bipedal robots, Extreme Mech. Lett. 42 (2021) 101076.
[37] M. Safartoobi, M. Dardel, H. Mohammadi Daniali, Gait cycles of passive walking biped robot model with flexible legs, Mech. Mach. Theory. 159 (2021) 104292.
[38] M.H. Korayem, S.F. Dehkordi, Derivation of motion equation for mobile manipulator with viscoelastic links and revolute–prismatic flexible joints via recursive Gibbs–Appell formulations, Robot. Auton. Syst. 103 (2018) 175-198.
[39] P. Doosti, MJ. Mahjoob, B. Dadashzadeh, Finite-time control strategy for the running of a telescopic leg biped robot, J Brazil Soc Mech Sci Eng. 41 (4) (2019) 196.
[40] S. S. Rao, Vibration of continuous systems, John Wiley & Sons, New Jersey, 2007.
[41] G. G. Muscolo, C. T. Recchiuto, Flexible Structure and Wheeled Feet to Simplify Biped Locomotion of Humanoid Robots, Int. J. Humanoid Rob. 13 (04) (2016) 1650030- 1: 1650030- 26.
[42] M. Dardel, M. Safartoobi, M.H., Pashaei, et al., Finite difference method to find period-one gait cycles of simple passive walkers, Commun. Nonlinear Sci. Numer. Simul. 20 (1) (2015) 79-97.
[43] I. Obayashi, S. Aoi, K. Tsuchiya, H. Kokubu, Formation mechanism of a basin of attraction for passive dynamic walking induced by intrinsic hyperbolicity, Proc. R. Soc. Lond. A Math. Phys. Eng. Sci. 472 (2190) (2016) 1-19.
[44] K. An, Q. Chen, A Passive Dynamic Walking Model Based on Knee-Bend Behaviour: Stability and Adaptability for Walking Down Steep Slopes, Int. J. Adv. Robot. Syst. 10 (365) (2013) 1–11.
[45] T. McGeer. Passive dynamic biped catalogue. In R. Chatila and G. Hirzinger, editors, Proc., Experimental Robotics II: The 2nd International Symposium, pages 465–490, Berlin, 1992. Springer–Verlag.
[46] H. Gritli, N. Khraeif, S. Belghith, Period-three route to chaos induced by a cyclic-fold bifurcation in passive dynamic walking of a compass-gait biped robot, Commun. Nonlinear Sci. Numer. Simul. 17 (11) (2012) 4356-72.
[47] M. Safartoobi, M. Dardel, M.H. Ghasemi, H.M. Daniali, Determination of the initial conditions by solving boundary value problem method for period-one walking of a passive biped walking robots, Robotica 35 (1) (2017) 166-188.